NTNU
Norwegian University of
Science and Technology

Alternating Current Corrosion of Carbon Steel

Eirik Belland

Materials Science and Engineering
Submission date: July 2011
Supervisor: Kemal Nisancioglu, IMTE
Co-supervisor: Sven Morten Hesjevik, Statoil Rotvoll

Norwegian University of Science and Technology
Department of Materials Science and Engineering

Preface

I hereby declare that this master thesis has been written in compliance with the regulations concerning examination of graduate students. The work has been carried out independently at the Norwegian University of Science and Technology (NTNU), Department of Materials Science and Engineering.

Furthermore I want to thank my thesis supervisors, professor Kemal Nisancioglu and Sven Morten Hesjevik for guidance in the preparation of this master thesis. I also want to thank Kjell Røkke for all the help concerning the equipment needed preparing this thesis. Last, but not least I want to thank professor Kemal Nisancioglu for including med in the corrosion group were I have gained a lot of new friends.

Trondheim, July 2011

Eirik Belland

Abstract

The objective was to investigate if the established theory concerning corrosion calculations and electrochemical behavior of carbon is valid when steel is exposed to AC in an electrolyte consisting of 3,5 wt% NaCl and distilled water. The experimental work was divided in two main parts.

The first part concerned corrosion testing, including weight loss measurements in stagnant conditions in combination with linear polarization resistance experiments. AC-current densities investigated was 0-, 50-, 75-, 100-, 150-, 220- and 500 A/m^2. Polarization curves were produced on two weight loss samples, one exposed to 150 A/m^2 and the other exposed to 220 A/m^2, at the end of the weight loss experiments.

From the corrosion testing it was found that the estimated corrosion current densities (i_{corr}) from the weight loss experiments on samples exposed to AC-current densities below 500 A/m^2, was in an approximate accordance with the i_{corr} values estimated from LPR. At 500 A/m^2 the measured corrosion rates and corresponding corrosion currents were slightly higher than the remainder. The higher corrosion rate measured from the samples exposed to 500 A/m^2 is suggested related to a non-faradaic corrosion contribution. The suggested mechanism is a facilitation of grain boundary corrosion at high AC-current densities leading to the loss of grains. This being a non-faradaic corrosion contribution it is not possible to measure with LPR or polarization curves.

The constant B [mV] from the Stern-Geary equation was estimated on basis of LPR measurements. The constant displayed a decreasing trend with increasing AC-current densities. This was explained by the lowering of anodic and cathodic tafel slopes with increasing AC-current densities. The polarization resistance (R_p' - [$\Omega \cdot m^2$]) also showed a decreasing trend with increased AC-current densities. This was explained by the increased current response in the LPR measurements with increasing AC-current densities.

The second part was intended to elucidate the effect of AC on electrochemical behavior of the carbon steel through producing polarization curves at different AC-current densities using a rotating electrode experimental setup. Alterations in corrosion current densities, cathodic tafel slopes, limiting current density of oxygen reduction and corrosion potentials on steel without AC and at current densities of 100-, 150-, 220- and 500 A/m^2 are investigated during the electrochemical testing.

From the rotating electrode experiments no significant change in corrosion current was found with increasing AC-current densities. The potential range, in which limiting current of oxygen reduction (i_{lim}) appeared, decreased with increasing AC-current densities. This decrease in i_{lim} also affected the corrosion potentials (E_{corr}). A decrease in the potential range of i_{lim} leads to a more cathodic E_{corr}. A particular observation was found at AC-current densities of 150 A/m^2 were the effect of i_{lim} seemed absent. The samples exposed to this AC-current density also attained the most cathodic corrosion potentials at approximately ~-850mV_{SCE} which was between 200-400mV lower than the samples exposed to the remaining AC-current densities. Cathodic tafel slopes showed a decreasing trend with increasing AC-current density. Anodic rafel slopes were considered absent due to pitting above E_{corr}.

Pictures of the weight loss samples were captured in the SEM. It was found that the formation of pits occurred on all weight loss samples exposed to AC. On the samples without induced AC no sign of pitting was observed. Hence it was found that the corrosion attacks attained a more local character when AC-current was induced in the steel samples.

List of contents

1. Introduction

For several decades AC corrosion has been a considerable problem in steel structures subjected to AC signals. Stray currents from power cables or electrical installations in the vicinity of pipelines make the steel prone to AC corrosion. Buried pipelines are commonly exposed to stray currents from high voltage transmission lines causing the steel to corrode in an uncontrollable manner. A similar problem arises when the steel is directly subjected to an induced AC signal. Statoil employs DEH (Direct Electric Heating) to avoid hydrate formation during a production stoppage. The DEH system heats the pipeline by inducing an AC signal in the pipeline. As a consequence the temperature of the pipeline is controlled by utilizing the heat generated by the resistive losses in the steel. Statoil has experienced AC corrosion at coating holidays as a result of the DEH system.

Several studies concerning AC corrosion have been published during the last decades, but the results of these studies are often contradictory and a satisfactory explanation of the AC corrosion mechanism is still not available. The objectives of this thesis are to elucidate the alteration in electrochemical behavior of carbon steel with induced AC, and investigate whether conventional corrosion rate calculations based on electrochemical testing apply for carbon steel exposed to AC.

2. Theoretical background

2.1 Previous work

Electrochemical behaviour

Overpotential behaviour

Bolzoni (2003) et al. discussed an AC corrosion mechanism related to anodic and cathodic overpotentials. It was suggested that the DC potential of a cathodically polarized metallic sample will increase when the cathodic process is oxygen reduction or hydrogen evolution. In cases of hydrogen evolution, the increase in DC potential is related to an overpotential reduction. In cases of oxygen reduction, the DC potential increase may be related to the increase in the limiting current density of oxygen diffusion due to the temperature increase that takes place at the metal-solution interface. Figure 2.1 illustrates the effect of AC on anodic overpotentials. Figure 2.2 displays the effect of AC on cathodic ocerpotentials. [1]

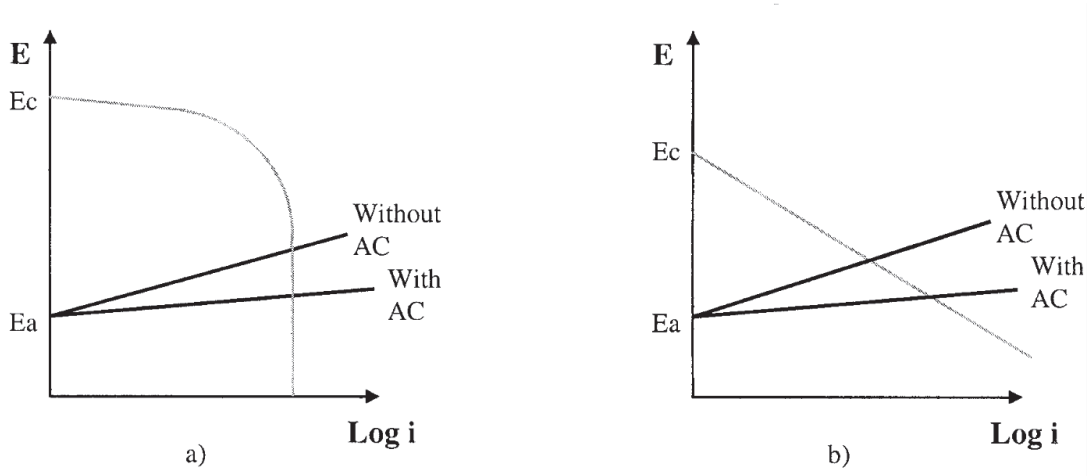

Figure 2.1: Schematic view of the effect of alternating current on anodic overpotential: a) Cathodic process is oxygen reduction; b) Cathodic process is hydrogen evolution. Figure from Bolzoni (2003) et al.[1]

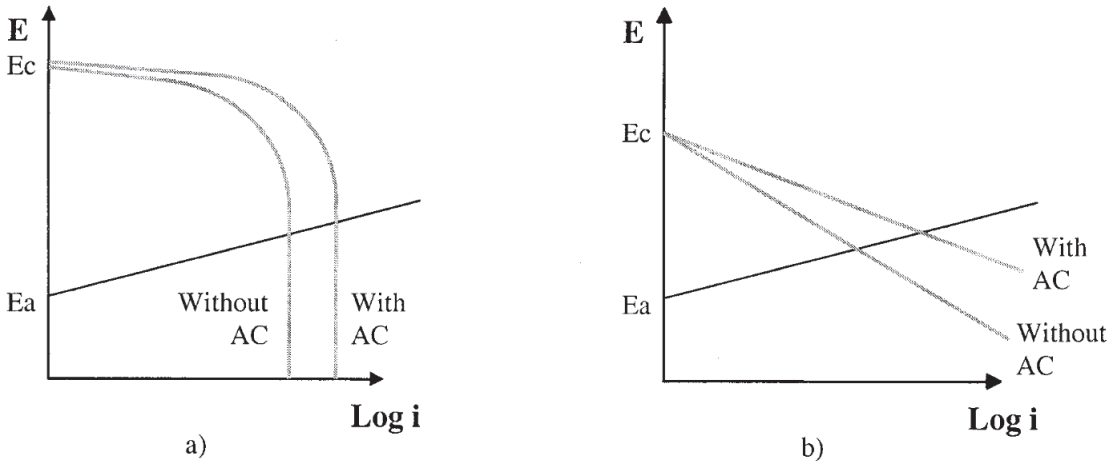

Figure 2.2: Schematic view of the effect of AC current on cathodic overpotential. a) Effect on oxygen reduction. b) Effect on hydrogen evolution. Figure from Bolzoni (2003) et al.[1]

A study conducted by Stamnes (2010) investigated the influence of AC on limiting current of oxygen reduction during polarization experiments. Bolzoni (2003) et al. suggested that the increase in DC potential in the cases of oxygen reduction was related to the increased limiting current density of oxygen diffusion. Stamnes' results contradict this by showing the limiting current density is unaffected by alternating current. However the potential range in which limiting current density appear decrease.[2] Figure 2.3 depicts how limiting current density is affected by a superimposed alternating current.

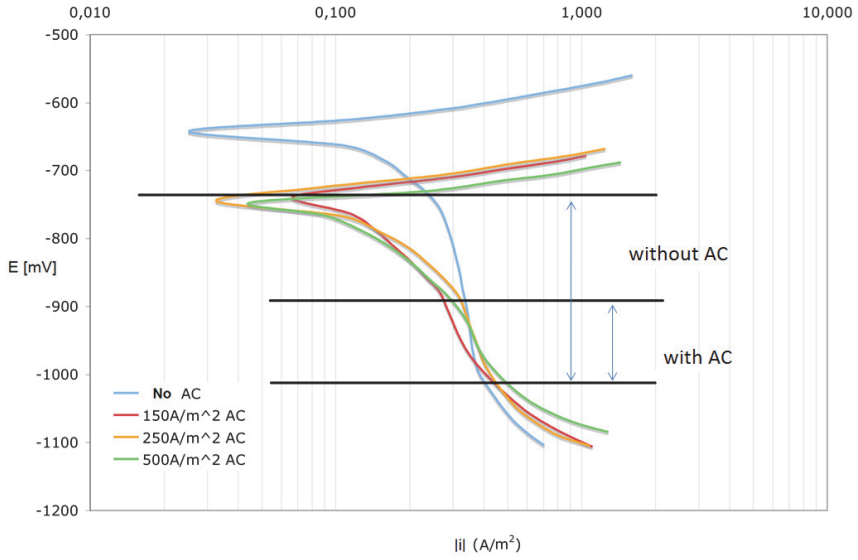

Figure 2.3: Range of limiting current decrease with induced AC while limiting current density remains unaltered. Modified figure from Stamnes (2010) [2].

Influence on corrosion potential

Studies have shown that corrosion potentials for carbon steels decrease to more cathodic potentials when exposed to alternating current. [2-5] The influence of AC on corrosion potential is depicted in Figure 2.4.

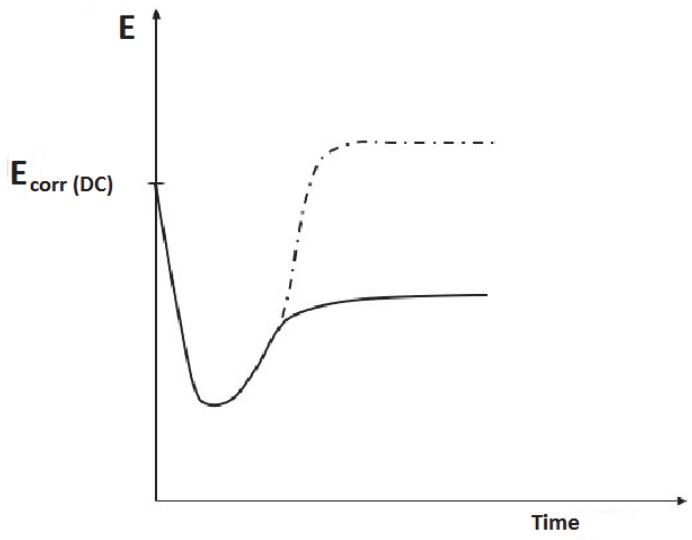

Figure 2.4: Schematic view of the influence of an AC signal on the corrosion potential. Figure from Stamnes (2010)[2].

From figure 2.4 it is observed that corrosion potential may change with induced AC. The magnitude of which AC influences open circuit potential and E_{corr} is related to the material and electrolyte. The solid line represents the behavior of carbon steel in a chloride containing electrolyte. The corrosion potential of carbon steel in a NaCl electrolyte has been reported to drop increasingly with increasing amplitude of the alternating current. Stabilizing time of corrosion potentials have been reported to last between 1 and 12 hours.[4]

Influence on corrosion rate

Pagano and Lalvani (1994) suggested a mechanism describing the rapid potential drop and the following stabilization of the corrosion potential. The surface is believed to activate when exposed to alternating current followed by a repassivation mechanism related to a pH effect in the double layer. Immersion experiments conducted for 48 hours at various applied AV implies decreasing corrosion rate with increasing pH. [5]

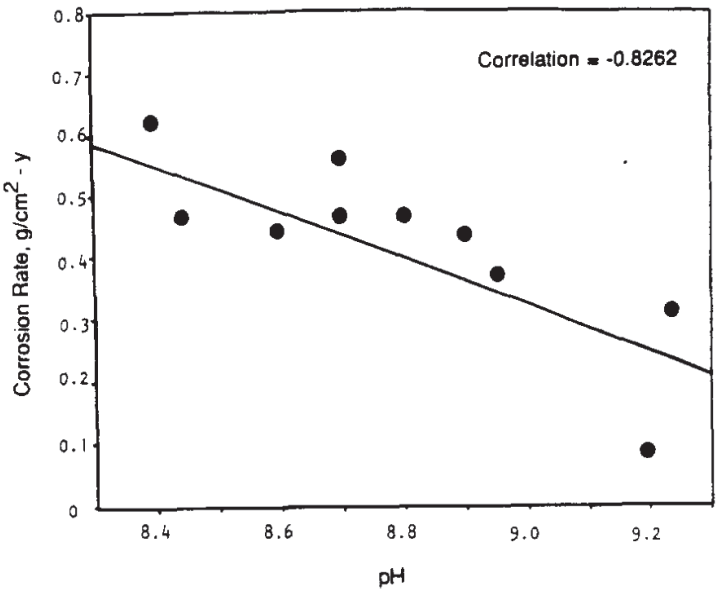

Figure 2.5: Corrosion rate as a function of pH. Figure from Pagano (1994) et al. [5]

Too further understand this phenomenon Pagano and Lalvani produced polarization curves at different pH values. The polarization curves showed a decrease in corrosion current with increased pH in bulk solution. A passivation area appears in the curves with pH levels above 8,2. Inadequate de-areation was suggested for the high initial corrosion potential for pH of 12. The polarizations curves in Figure 2.6 support the theory of a passivating effect of pH.

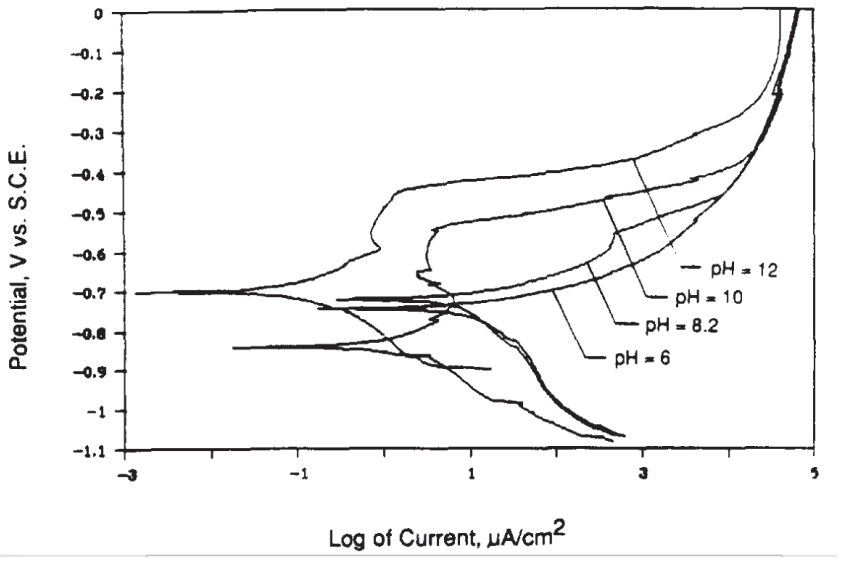

Figur 2.6: Potentiodynamic polarization curves for carbon steel in simulated seawater at different pH levels. Figure from Pagano (1994) et al. [5]

In early studies it was believed that the AC corrosion process could be controlled to negligible levels using cathodic protection applied according to industrial standards. However in 1986 an incident of AC corrosion at a coating defect was encountered. This occurred despite the CP system working satisfactory. A threshold AC current density of 100A/m^2 on a 1cm^2 coating defect was suggested to ensure sufficient protection against AC induced corrosion. It was found that the highest AC corrosion rate occurred on a 1cm^2 coating holiday. [6] However Mark Yunovich (2004) reported increased corrosion rates at AC-current as low as ~20 A/m^2. [7] At high AC-current densities (500 A/m^2) the corrosion attack was worse using cathodic protection (CP) than without CP. This observation is in accordance with L.V.Nilsen's (2004) observations regarding an increase of corrosion rates due to alkalization of the environment in the vicinity of a coating holiday when the steel is subjected to high AC-current densities (500 A/m^2) and is cathodically protected. [8]

The effect of frequency

Studies have shown that increasing AC frequency decrease corrosion rates.[5, 9, 10]

Figure 2.7 depicts an equivalent electric circuit representing the three impedances occurring in a corrosion process. C_{dl} is the capacitance of the double layer, R_s is the resistance in the electrolyte and Z_p is the non-linear polarization impedance. Z_p and C_{dl} are in parallel and in series with R_s. Equation 2.1 shows that the total current density, i, is decomposed into faradaic current density, i_f, and double layer capacitance current density, i_{dl}. Only the faradaic current contributes to the electrochemical corrosion process.

$$i = i_f + i_{dl} \tag{0.1}$$

Direction of current flow is determined by the magnitude of the polarization- and capacitor impedance. The current tends to flow through the impedance with least resistance. Since the faradaic current is the only current contributing to the corrosion process, the corrosion rate depend on the double layer impedance. Impedance of a capacitor is a function of frequency, f, and double layer capacitance, C_{dl}. Impedance of the double layer is expressed in eq. (2.2)

$$Z_{Cdl} = \frac{1}{2\pi \cdot f \cdot C_{dl}} \tag{0.2}$$

Eq. (2.2) shows that increasing frequency decreases the double layer impedance. At high frequencies the majority of the current contribute to charging and discharging of the double layer leaving the faradaic current contribution negligible. Hence current transfer trough the double layer is believed to be a determining factor in the AC corrosion process.[10]

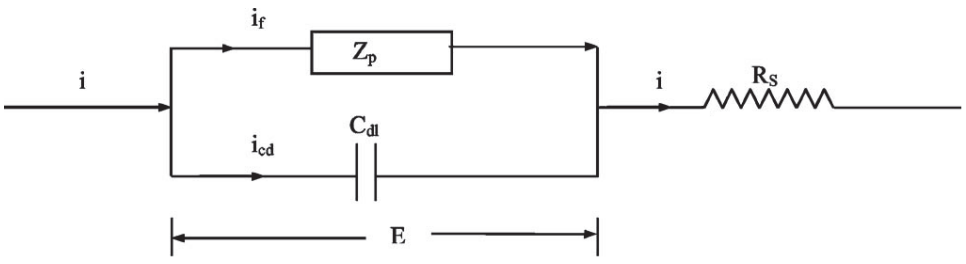

Figure 2.7: Schematic of elements involved in corrosion of a metal specimen subjected to an AV/AC in an aqueous environment. Lalvani (2008) et al. [10]

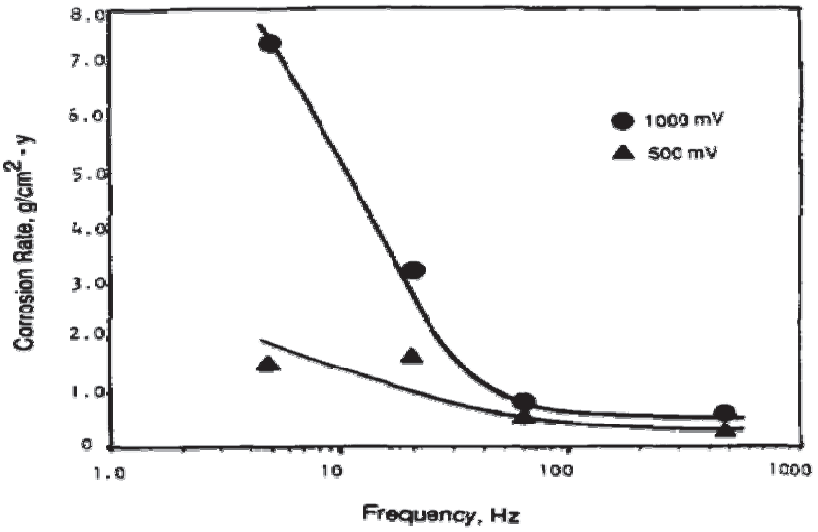

Figure 2.8: Corrosion rate decrease with increasing AC frequency. Figure from Pagano (1994) et al. [5]

In 1994 Pagano et al. studied the effect of frequency on corrosion rate of mild steel in seawater. The observed decrease in corrosion rate with increase in frequency is related to the decrease in the double layer impedance making the polarization impedance the main current carrying component.

The effect of an AC signal on oxide formation

Formation of a dark oxide surface film has been reported as a result of AC in alkaline environments. Magnetite is the suggested oxide film being formed. There is no certainty concerning the oxide film's influence on corrosion rate. However the film formation seems to appear independent of corrosion rate[2, 11, 12]

In 1998 Bosch and Bogaerts performed a theoretical study concerning AC-induced corrosion considering diffusion phenomena. The study distinguished between the two cases; anodic and cathodic reactions under activation control and under mixed control. The influence of AC-induced voltages on corrosion behavior was reported to be strongly dependant on the Tafel-parameters. The increase of corrosion rates when cathodic reactions are under mixed control was determined to be limited by the diffusion-limited current density through numerical analysis. Figure 2.9 shows a lowering of the corrosion potential, increase in corrosion rates and that the cathodic reactions become diffusion-limited with increasing induced AC voltage. [13]

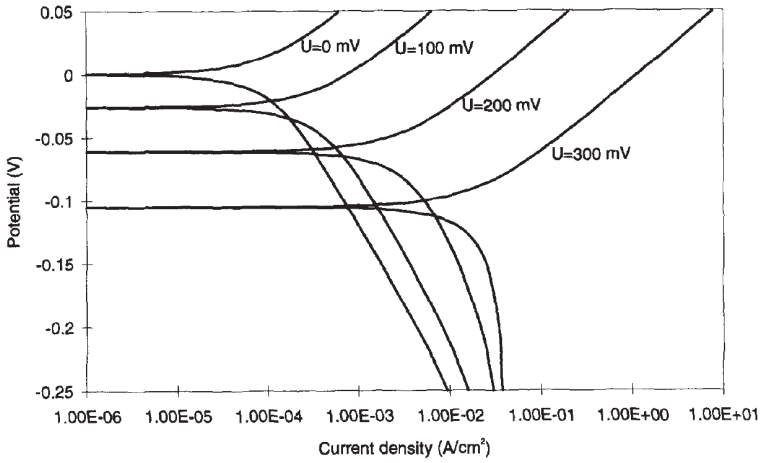

Figure 2.9: Simulated polarization curves. $i_{corr} = 10^{-4}$ A/m^2, b_a = 60mV/dec, b_c = 120mV/dec. Figure from Bosch and Bogaerts [13]

2.2 Preliminary project work

During autumn 2010 a preliminary project work was carried out developing the experimental testing equipment. The solution was to use an electric circuit consisting of two networks introducing AC and DC in the working electrode and utilizing separate counter electrodes for the separation of the AC-net and DC-net respectively. A capacitor was used in the AC net to avoid DC signals from circulating in the AC net. In the DC net an inductance was implemented to provide stable DC measurements during polarization experiments. The equipment and its electrical circuits are explained more comprehensively in the chapter 3 -Experimental work. Additionally polarization curves at stagnant conditions were produced at 0, 150 250 and 500 A/m^2. A lowering of tafel curves was observed and a passivating area close to the corrosion potential appeared to occur. Also a black oxide layer on the sample surface after polarization experiments with induced AC.[12]

3. Experimental

The objective of the experimental work was to investigate whether the established theory concerning electrochemical behavior of carbon steel in a salt water electrlyte apply when exposed to induced AC. Weight loss measurements at various AC-current densities were carried out and compared to polarization curves and linear polarization resistance measurements.

3.1 Material specification, electrolyte and reference electrode

Material specification

The material used in the experiments was carbon steel. Chemical composition was determined by optical emission spectroscopy using a Spectro Spectromax. Table 3.2.1 shows the average chemical composition of the steel. Appendix A includes data measurement sheets from the optical emission spectroscopy.

Table 3.1.1: Average chemical composition

Wt% C (Average)	Wt% Mn (Average)	Wt% P (Average)	Wt% S (Average)
0,01025	0,23435	0,00545	0,00765

Electrolyte

The electrolyte used in the experiments consisted of distilled water with 3,5 wt% dissolved NaCl. The water was distilled using Millipore Elix distiller. Sodium Chloride (grade ACS,ISO,Reag. Ph Eur) was delivered by Merck.

Reference electrode and salt bridge

All reported DC-potentials in this thesis are given in reference to the saturated calomel electrode (SCE). T The calomel electrode (REF-401) showed in figure 3.1.1 was delivered by “Radiometer Analytical”. The reference electrode was separated from the electrochemical cell using a beaker filled with saturated KCl. Galvanic connection was attained by using a salt bridge. The KCl electrolyte for the SCE was replaced prior to each experiment. Agar-solution was used in the salt bridge. This separated the electrolytes and maintained conductivity. The Agar-solution was made using Agar starch and 3M KCl. The salt bridge used in the polarization experiments was custom-made to fit the electrochemical cell. Figure 3.1.2 shows the two types of salt bridges used in the experiments. All salt bridges utilized a luggin capillary to prevent large ohmic drops. To

avoid chloride contamination in the electrochemical cell, the NaCl electrolyte level was kept slightly above the KCl electrolyte. This height difference should be kept at a minimum to avoid NaCl to contaminate the KCl electrolyte. . Figure 3.1.3 is a schematical view of the height difference needed and depicts how the reference electrode is galvanically connected to the electrochemical cell using the salt bridge.

Figure 3.1.1: Reference electrode used in the weight loss experiments

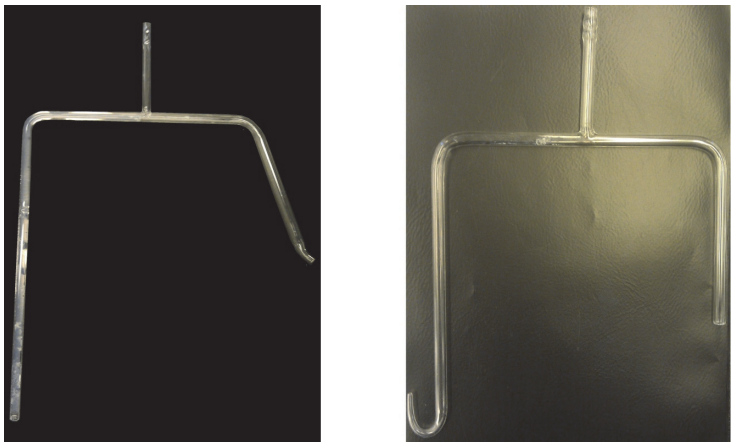

Figure 3.1.2: Salt bridges used in the polarization experiments (left) and in the weight loss experiments (right).

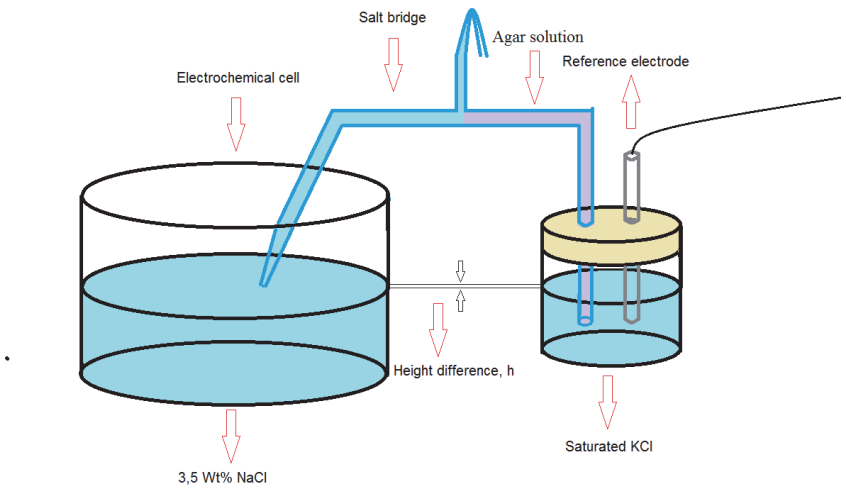

Figure 3.1.3: Schematic view of the height difference needed to avoid KCl contamination of the 3,5 wt% NaCl electrolyte.

Standard hydrogen electrode (SHE)

Due to environmental issues concerning the mercury containing saturated calomel electrodes (SCE) the use of standard hydrogen electrodes (SHE) was desired. The SHE showed in figure 3.1.4 was custom-made for the experiments in this study. This particular hydrogen electrode is supposively is easy to prepare and use. It required 1M hydrochloric acid (HCl) and hydrogen gas at atmospheric pressure in contact with a platinum mesh inside the SHE. The hydrogen gas was produced by imposing a potential difference of -2,2 V between the platinum mesh in the SHE and a platinum counter electrode. However during the polarization experiments the SHE was unable to attain stable potential measurements. This in addition to the possibility of acidification of the electrolyte, the SHE was regarded as incapable of providing adequate reference potential measurements. Figure 3.1.4 shows the SHE before and after assembly.

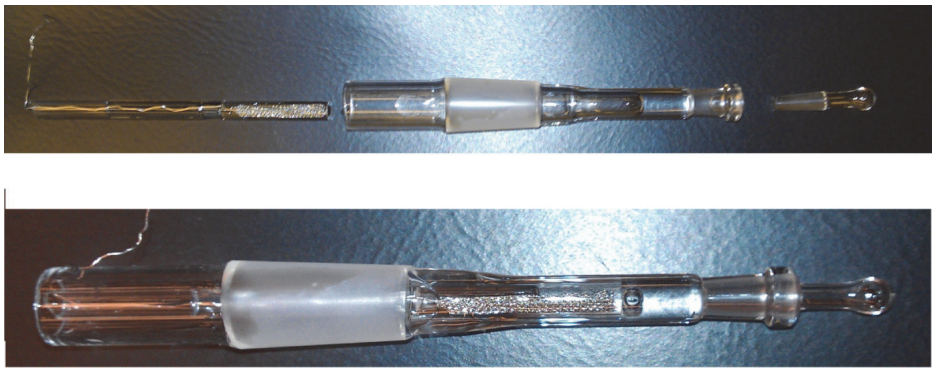

Figure 3.1.4: SHE before assembly (top picture) and after assembly (bottom picture).

3.2 Corrosion testing

Weight loss measurements

Three identical weight loss experimental setups were made to be able to run simultaneous weight loss experiments with different AC current densities. Figure 3.2.2 shows one of the setups used for the weight loss measurements. The reason for this was to avoid AC-current interference between the samples. The different setups were tested prior to the experiments to ensure equal electrochemical behavior of the different setups. All weight loss experiments were carried at open circuit potential (OCP).

Sample dimensions and preparation

Dimensions of the weight loss samples: Thickness = 2 mm, length = 80 mm, width = 20 mm. The exposed immersion area after painting was 6,5 A/m^2. Initially the exposed area was intended to be larger, however this proved impossible due to the VariAC was unable to impose a high enough voltage to attain AC-current densities of 500 A/m^2. Figure 3.2.1 shows the sample at different stages of the preparation procedure. The samples were ground to a 1000 grit finish and cleaned with acetone, ethanol and distilled water before drying with a heat gun drier. Subsequently the samples were weighed, masked and painted. The samples where rinsed with acetone and ethanol prior to weighing and painting. The coating used in the experiments was "Microshield – Stop-off lacquer" After painting the samples were set to dry for at least 24 hours.

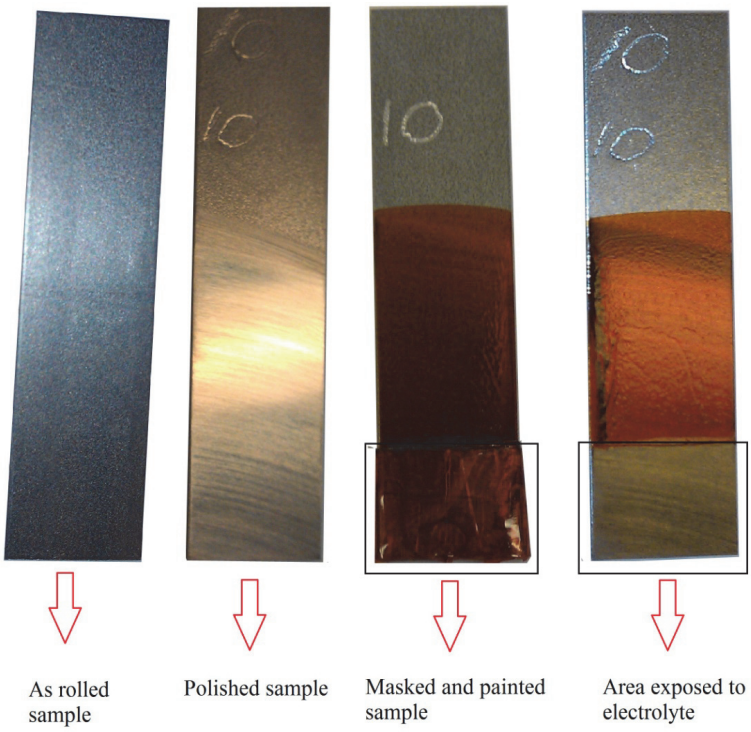

Figure 3.2.1: Figure showing the different steps of the sample preparation.

Weight loss measurement apparatus

The weight loss apparatus was almost identical to the polarization sweep setup. However the potentiostat used was a manual Bank-MP81, the experiments was carried out in stagnant conditions, and an Agilent data logger was introduced. The apparatus is further explained in the "Electric circuit" section.

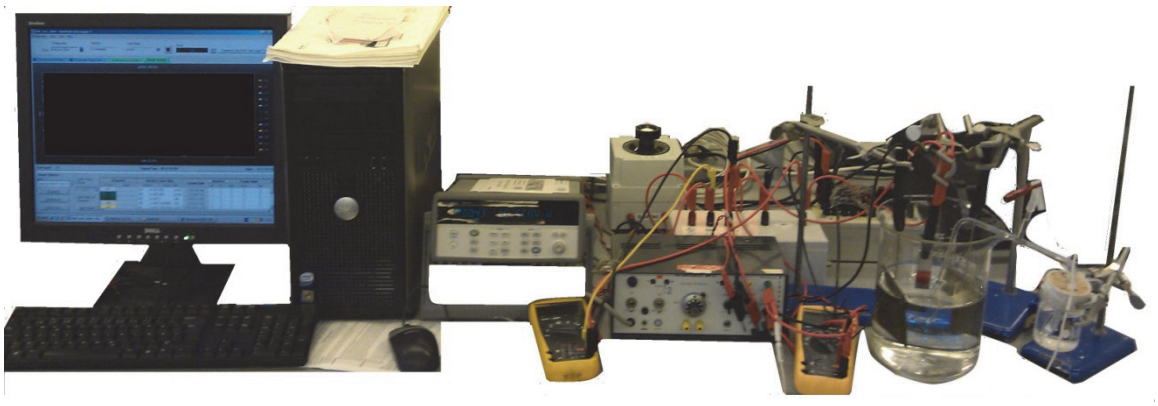

Figure 3.2.2: One of three weight loss experimental setups.

Linear polarization resistance (LPR)

All weight loss setups were connected to a Bank MP-81 manual potentiostat. This enabled the possibility of carrying out LPR-(Linear Polarization Resistance) measurements. The sample was polarized ± 10 mV from OCP, the current response was logged and $1/R_p$ values were calculated. ΔE was considered to be within the limits for which the linear relationship between I_{corr} and ΔE/ΔI. ΔE was corrected for IR-drop. Samples exposed to AC-current delivered unstable instantaneous current readings. Hence all the samples were polarized ± 10 mV for 30 seconds prior to logging.

Removal of corrosion products

To attain weight loss measurements the corrosion products had to be removed. An inhibited hydrochloric acid solution was made according to the ASTM G1 standard. The inhibitor used was hexamethylene tetramine delivered by ROTH. The solution was made up by adding 0,5 litre consentrated HCl (% > 37) slowly into pre-mixed 0,5 litre distilled water and 3,5 grams inhibitor. The samples were submerged in the solution one with one minute intervals until the corrosion products were completely removed. Inevitably some of the base material was removed during the procedure. Hence identical weight loss procedures were carried out with a clean and equally prepared control sample. The weight losses were measured with the immersion time intervals corresponding to the actual weight loss samples. The weight losses measured for the control sample was corrected for in the corroded samples making the weight loss measurements more reliable.

3.3 Electrochemical testing

Sample specification and sample holder

The sample is a cylinder with an outer diameter of 12 mm and a height of 7,97 mm exposing a surface area of 3 cm^2. The shaft used in the experiments was delivered by Pine Reasearch instrumentations. However the steel samples, seals and seating caps were custom-made to fit the electrochemical cell. To ensure satisfactory electrical conductivity the samples had to be machined with a high degree of precision. Sufficient conductivity was ensured by measuring the resistance between sample and the wire connected to the potentiostat. The sample holder is made from a stainless steel quality. To avoid galvanic coupling between the carbon steel sample and stainless steel shaft, no electrolyte is allowed to permeate into the sample holder. Hence high precision machining of seals and seating cap is also required. Figure 3.3.1 shows the sample and sample holder.

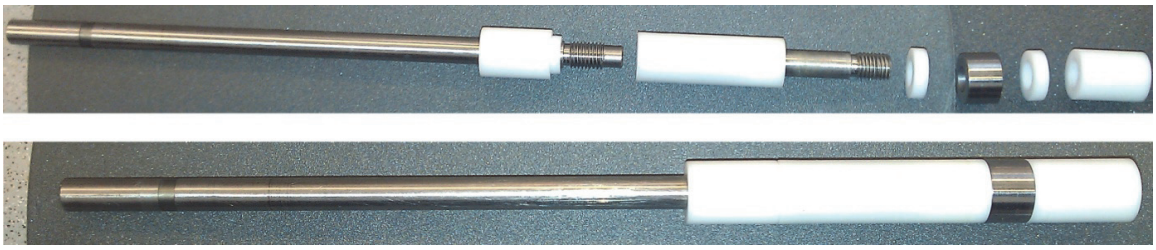

Figure 3.3.1: Picture of the sample and sample holder used in the rotating electrode experiments.

Apparatus

A computer controlled Gamry Reference 750 potentiostat was used for the polarization sweep experiments. The software used was Gamry Framework (version 5.51, program package DC105) using the potentiodynamic sweep program. To enable the possibility of observing limiting current of oxygen reduction (i_{lim}) a rotating electrode setup was used. Rotational speeds of 175- and 350 RPM to attain turbulence. Rotator was delivered by Pine instruments. Figure 3.3.2 shows the apparatus used in the polarization sweep experiments. A more comprehensive explanation of the apparatus is found in the “Electric circuit” part. To the left in figure 3.2.2, a water bath containing a heating element and a water loop for temperature control is shown. This equipment was not used for the

experiments in this thesis, however it is planned further work including temperature control during a project work autumn 2011.

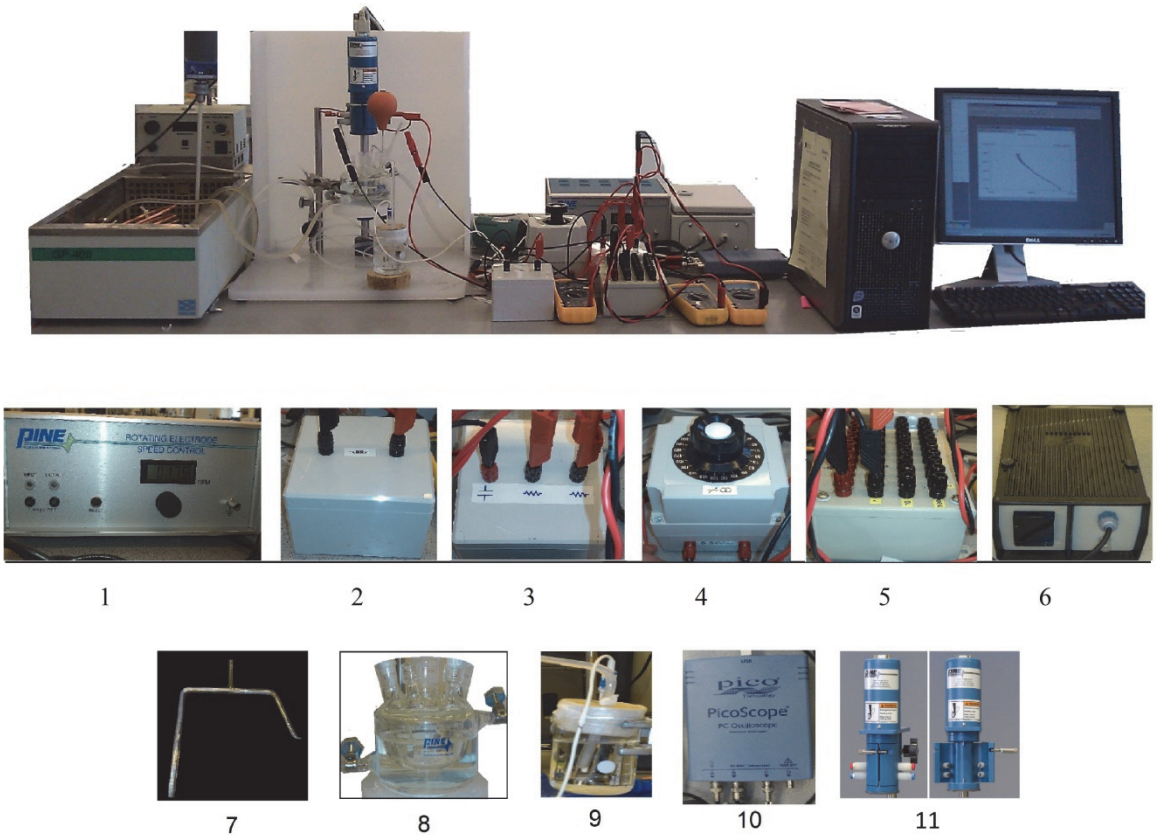

Figure 3.3.2: Apparatus used in the polarization sweep experiments.

Test procedure

Samples was ground to 1000 grit and rinsed with acetone and ethanol prior to the experiments. However the cylindric shape of the samples complicates the grinding procedure. An floor mounted electric drill was used for grinding of the samples. Samples were kept in an eksikator to prevent corrosion whenever not exposed to an experiment. All equipment in contact with the electrolyte was thoroughly rinsed with a degreasing agent and flushed with readily mixed 3,5 Wt% NaCl electrolyte prior to the experiments.

The experiments were initiated immediately after this procedure. The polarization sweeps were carried out with a sweep rate of -1 mV/sec. A potential range from -1200 mV_{SCE} to -450 mV_{SCE} was used for AC current densities of 500-, 220- and 150 A/m^2. Due to corrosion potentials of approximately -450 mV_{SCE} for the samples without AC and at 100 A/m^2, a sweep range from -1200 mV_{SCE} to -350 mV_{SCE} was used.

3.4 Electrical circuit

The electric circuits in polarization- and weight loss experiments are equal seen from an electrochemical point of view. The electrical circuit consisted of two networks, one AC-net and one DC-net respectilvely. The two networks were separated using two counter electrodes, one for the AC net (CE-AC) and one for the DC net (CE-DC). An AC power supply (VariAC) superimposed the desired AC-signal between the working electrode (WE) and the AC counter electrode (CE-AC). AC current was measured over a 10Ω resistor. A 500μF capacitor prevented DC from circulating in the AC net. In the DC net a potentiostat was used to polarize the steel (WE). DC current was measured over a resistor between the CE-DC and the potentiostat. A measuring resistor of 10Ω was used for the weight loss setups and a 1Ω resistor for the polarization experiments. The use of a **larger** resistor on the weight loss experiments was due to a need for a better resolution of the LPR measurements due to the small currents. The 1Ω resistor in the polarization experiments was utilized to observe if the current values from the Gamry potentiostat corresponded to the multimeter readings. A 10H inductance between the working electrode and potentiostat reduced the AC signal interference in the DC network thus providing stable DC measurements. This inductance represented a resistance of 9,3Ω, and the potential drop was corrected for in the calculations. Cables were twined were it was possible to reduce signal interference from the surroundings. To avoid any unwanted short circuits, and for safety reasons, the electrical equipment was kept at a common floating ground by using an isolating transformer as main current supply. DC potential of the steel sample (WE) was measured using a SCE reference electrode. Figure 3.4.1 depicts the electrical circuit used for the weight loss experiments.

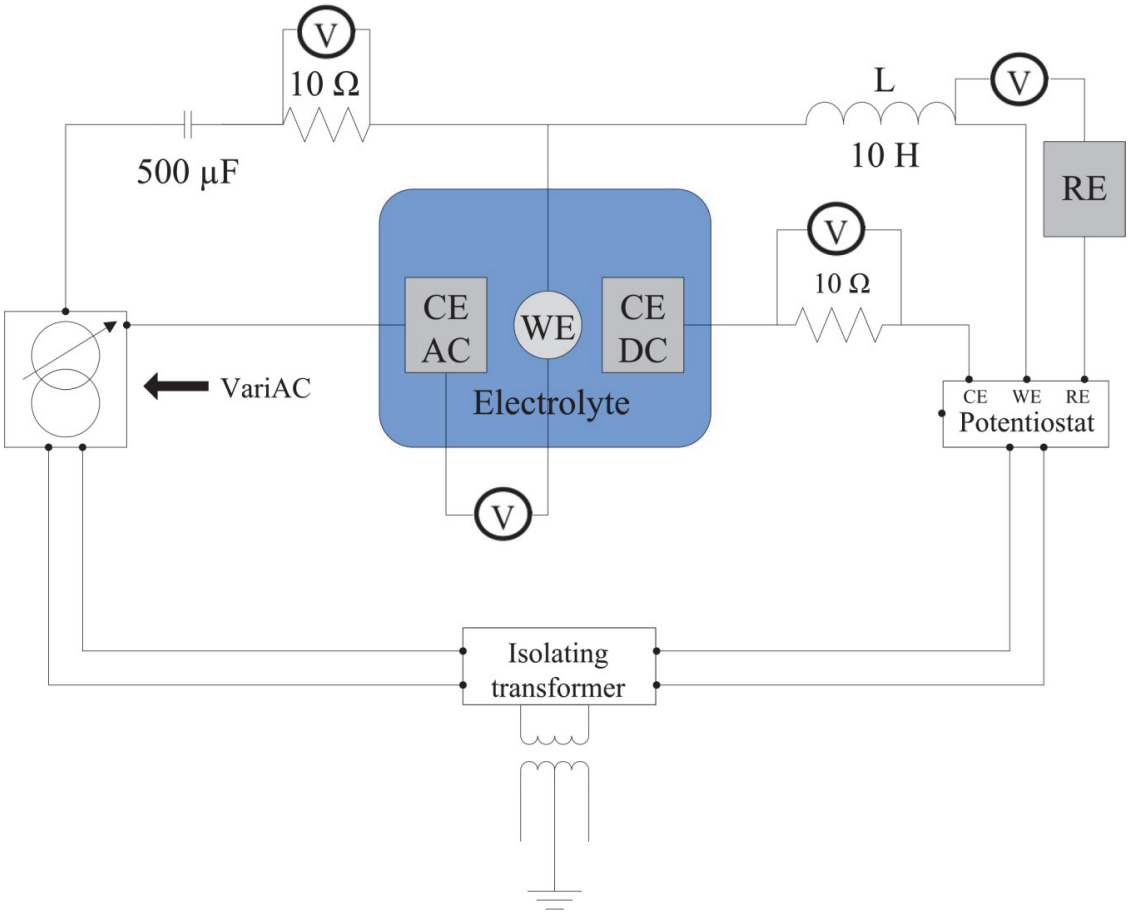

Figure 3.4.1: Schematical view of the electric circuit in the weight loss experiments.

The electric circuit used in the polarization experiments is equal to the weight loss setup, however an oscilloscope was introduced to obtain in-situ measurements of the alternating signals. This allowed investigation of a possible phase shift between AC-current and alternating cell voltage. Images from the oscilloscope were captured at approximately -1150 mV_{SCE}, at the corrosion potential and at approximately -450 mV_{SCE}. The implementation of the oscilloscope into the circuit was challenging due to severe signal interference on the oscilloscope measurements. A common ground was required to attain adequate measurements. The cables were arranged in such a manner that ground on all cables were connected to the WE on the right side of the resistor in the AC net. Figure 3.4.2 shows how the oscilloscope is connected to the circuit.

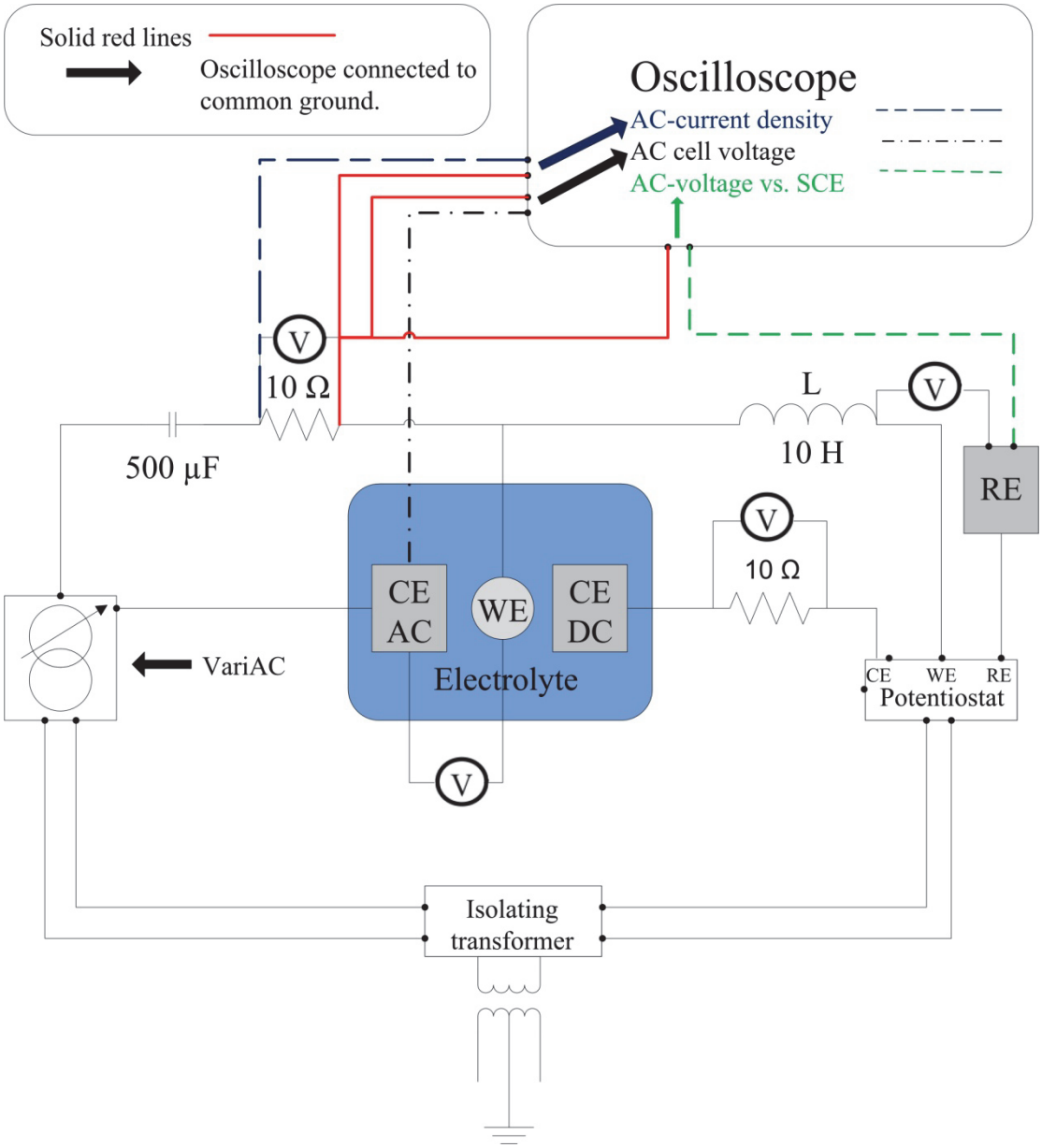

Figure 3.4.2: Schematic view of the electric circuit with oscilloscope for the polarization experiments.

3.5 Scanning electron microscope (SEM)

A Hitachi S-3400N low vacuum scanning electron microscope (LV-SEM) was used for investigation of the sample surfaces prior to and after the removal of corrosion products. An accelerating voltage of 15 kV, an approximate working distance of 10 mm. (WD) and the secondary electron detector (SE) was used.

4. Results

4.1 Corrosion testing

Weight loss (WL) measurements were carried to investigate the influence of AC-current of corrosion rate. The total immersion time for the displayed corrosion rate measurements adds up to 2611 hours.

Weight loss measurements

From the WL measurements showed in Figure 4.1.1 no significant correlation between corrosion rate and induced current density was encountered. A slight increase in corrosion rates are observed in the black columns from 100 A/m^2 and above compared to the sample with 0 A/m^2, 50 A/m^2 and 75 A/m^2. The red columns indicate that the samples were immersed for approximately 16 days compared to between 9 and 10 days for the remainder. The intention of the prolonged immersion time was to investigate a possible relation between a decrease in corrosion rate with increasing immersion times and high AC-current densities. Both for 220 A/m^2 and 500 A/m^2 a lower corrosion rate was measured for the extended immersion times. The only corrosion rate with induced AC-current density which stands out is at 500 A/m^2 and an immersion time of 9 days. This is the sole experiment which clearly indicates an increase of corrosion rate compared to the experiments without induced AC. Initially the intention was to perform two parallels for 0-, 100-, 150-, 220- and 500 A/m^2. By mistake two of the experiments were carried out at half the intended AC-current density. Hence experiments at 50- and 75 A/m^2 were measured instead of the second parallel with 100- and 150 A/m^2. The weight loss samples exposed to 50- and 75 A/m^2 experienced little, or no corrosion outside the intended exposure area compared to the remainder. This may be the reason for the lower measured corrosion rates. Figure 4.1.4 shows the sample exposed to 75 A/m^2 after the weight loss experiment.

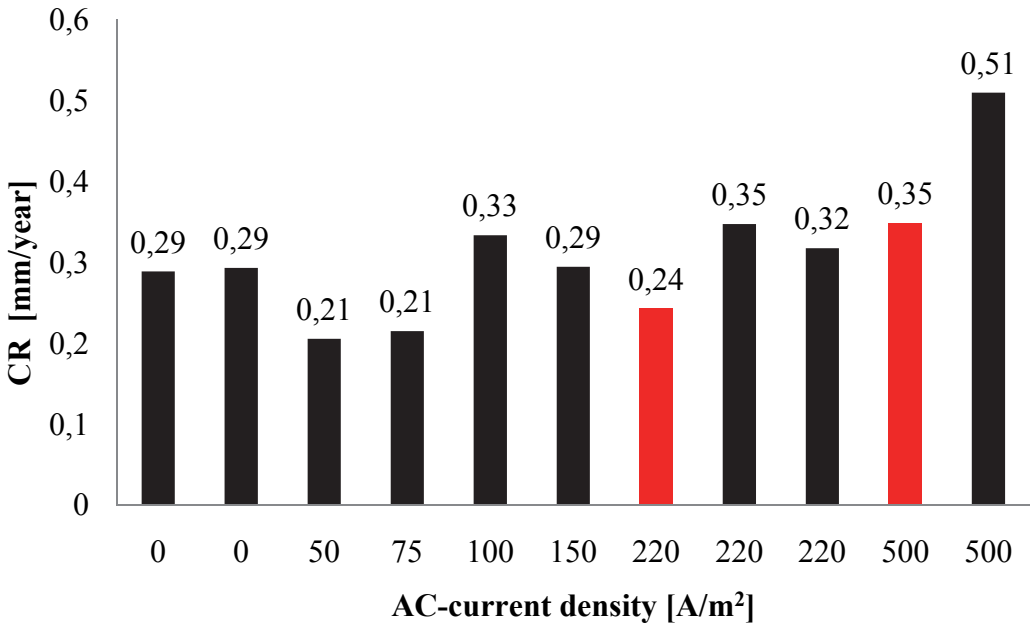

Figure 4.1.1: Corrosion rates at various AC-current densities

Unevitabely som base material will be removed during the corrosion product removal procedure. To correct for the additional weight losses, equally prepared and clean samples were immersed in the inhibited hydrochloric acid solution. The samples were immersed for the same time intervals as for the weight loss samples. Figure 4.1.3 shows the measured additional weight losses at the different immersion times. These weight loss measurements were subtracted from the total weight loss of the samples.

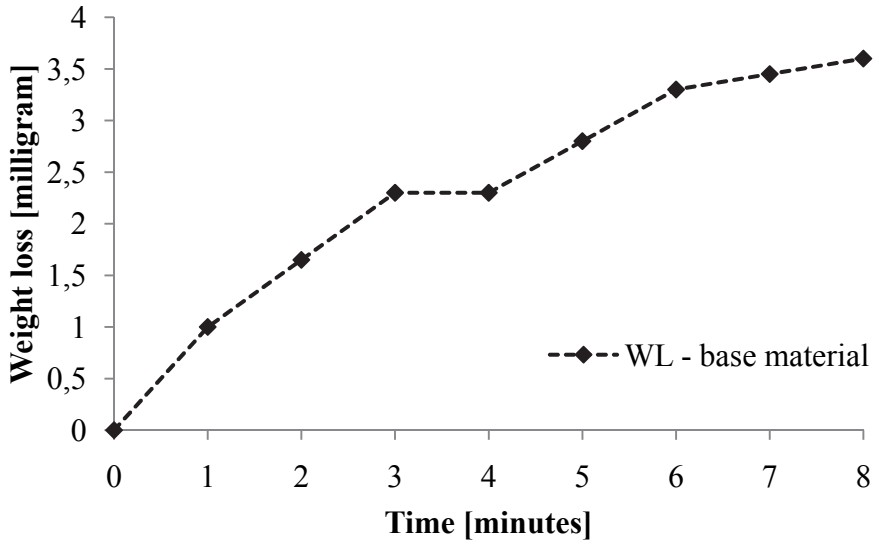

Figure 4.1.2: Measured additional weight loss at different immersion times.

Unfortunately the samples experienced corrosion outside the intended exposure area during the weight loss experiments. It is impossible to determine the severity of the attack and thus its influence on measured corrosion rates. It was however not observed any significant corrosion under the coating. The coating was also easy to remove using acetone. Hence the applied coating appeared to give a satisfactory protection of the steel during the weight loss experiments. Figure 4.1.3 shows an example of corrosion outside the intended exposure area, and the protecting effect of the coating.

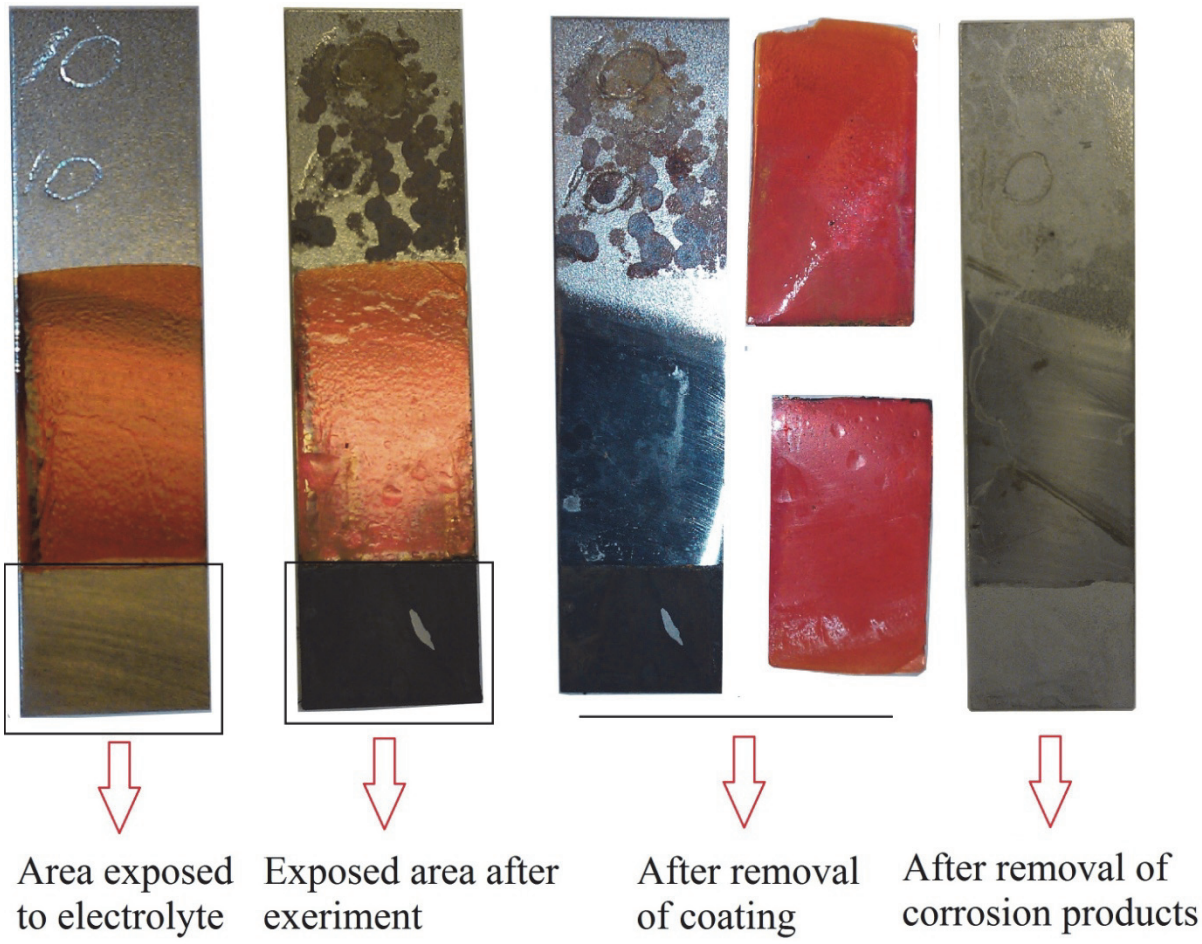

Figure 4.1.3: Sample exposed to 500 A/m^2 at different stages during the course of the experimental work. Notice the corrosion attack outside the intended exposure area.

In the last experiment (75 A/m^2) the entire sample was grinded to a 1000 grit finish. After the experiment the sample, showed in figure 4.1.4, appeared uncorroded except from the intended immersion area.

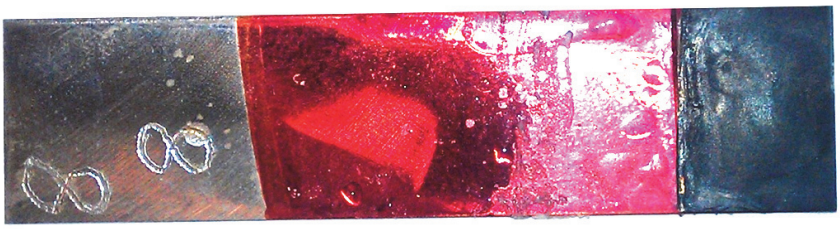

Figure 4.1.4: No, or little signs of corrosion outside the immersion area on the fully grinded sample (75A/m^2).

All samples with induced AC obtained a dark oxide layer as shown in Figures 4.1.3-4.The samples without induced AC gained an orange-red oxide layer.

Linear Polarization Resistance (LPR)

Linear polarization resistance measurements were carried out each day for one samples exposed to 0-, 50-, 75-, 100-, 150-, 220- and 500 A/m^2. One parallel (one sample on each AC-current density) of LPR measurements were produced. In the presented curves all the measurements from the weight loss measurements are included. Hence the larger amount of data points from the WL experiments in Figures 4.1.5-6. Estimations of B constants and corrosion current densities were based on average LPR values. Figure 4.1.8 shows R_p' transient to display how the polarization resistances at the various AC-current densities develop during the weight loss experiments.

Figure 4.2.6 shows the estimated corrosion current densities from WL measurements and LPR measurements. LPR corrosion current estimations were based on average R_p values and the corresponding constant B from Figure 4.1.6. The corrosion current densities estimated from LPR measurements did not vary between the different AC-current densities. However at an AC-current density of 500 A/m^2 the measured corrosion rates from the weight loss experiments seemed to increase.

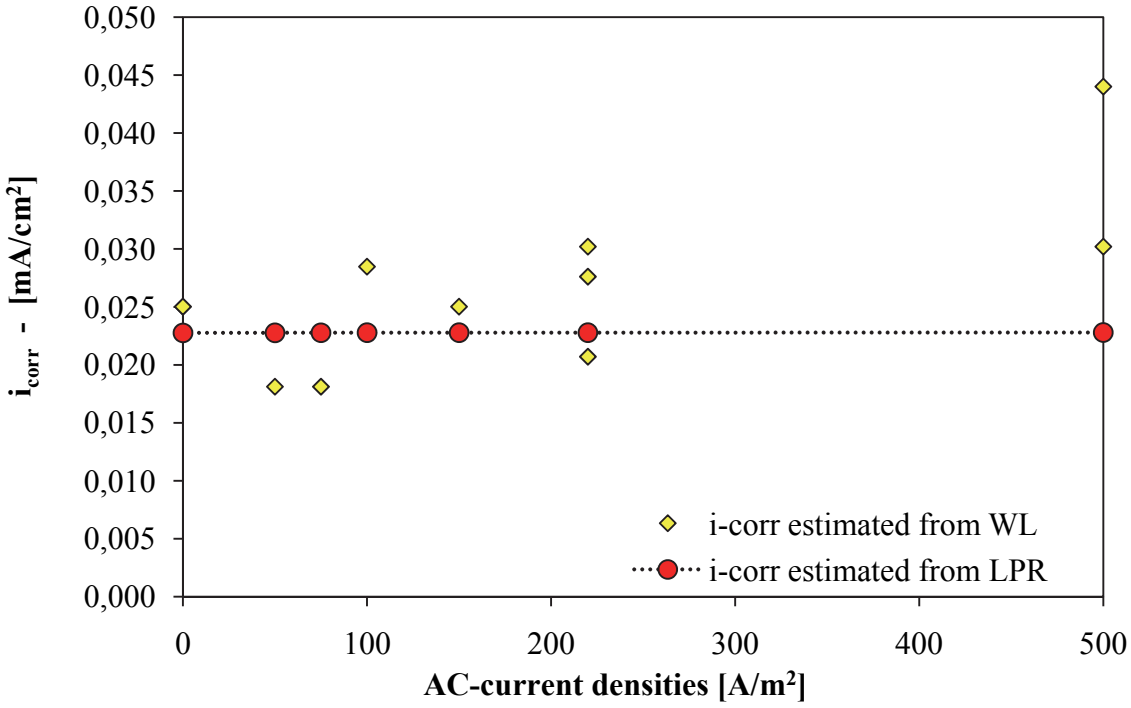

Figure 4.1.5: Corrosion current estimations at various AC-current densities based on weight loss measurements and LPR measurements.

Figure 4.1.6 displays the B constants estimated from weight loss measurements and LPR measurements at various AC-current densities. B estimated from LPR measurements was based on extrapolated tafel slopes. B estimated from the WL measurements was based on the corrosion current density (calculated from the corrosion rate) and the R_p' from the LPR measurements. The B constants appear to be of the similar value at low AC-current densities. However above 100 A/m^2 the B constants diverge making the value estimated from the WL measurements higher than from the LPR measurements.

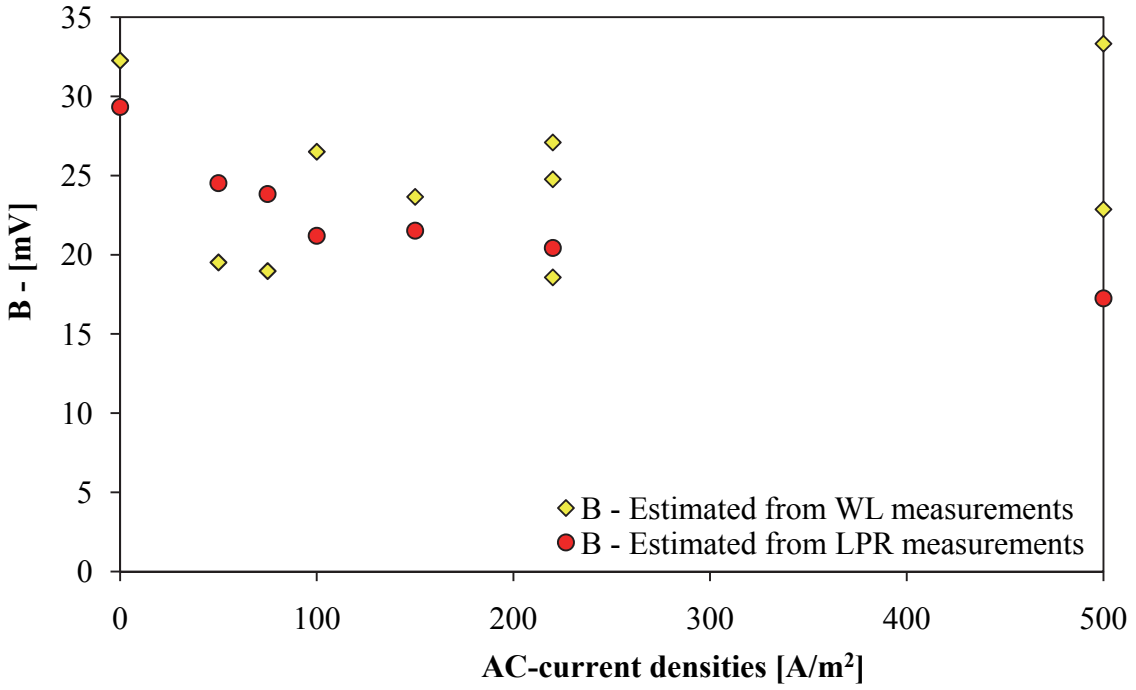

Figure 4.1.6: Estimations of the constant B at various AC-current densities based on weight loss measurements and LPR measurements.

Figure 4.1.7 shows the R_p' values polarization resistance transients at various AC-current densities. The R_p' value is the R_p multiplied with the surface area. R_p is estimated from the total measured currents, not current densities, and the 9,3Ω resistance introduced by the inductance is subtracted. The initial polarization resistances vary, however the R_p' values seem to stabilize after approximately 2-5 days. Higher AC-current densities appear to stabilize slower than the lower AC-current densities. In general a lowering of the polarization resistance is observed with increasing AC-current densities.

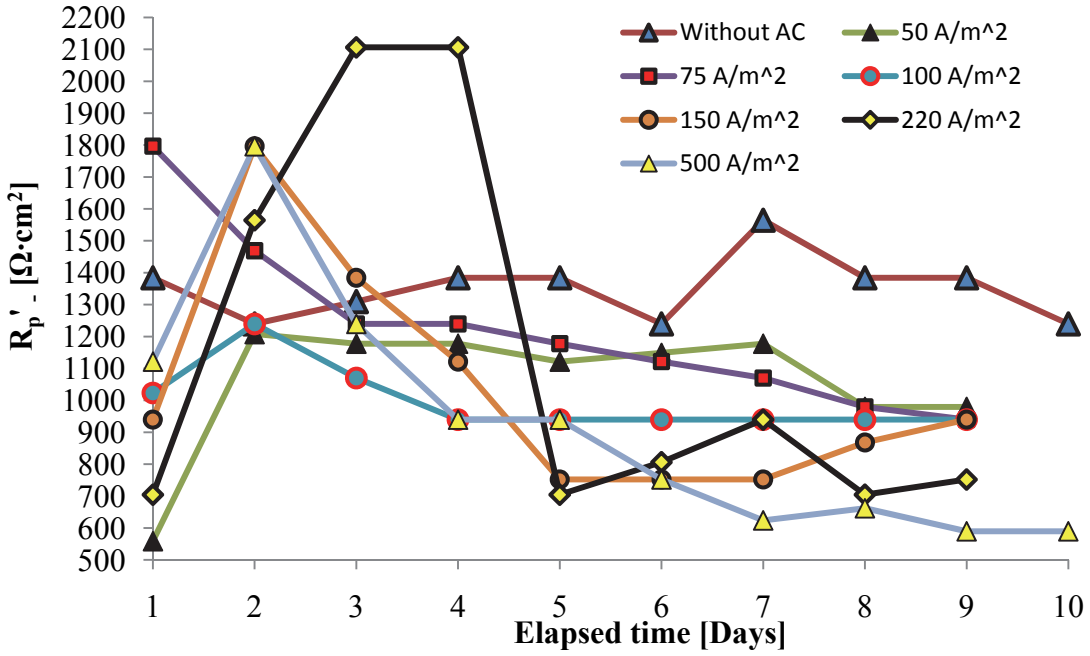

Figure 4.1.7: R_p' value transients at various AC-current densities calculated from the LPR measurements.

Polarization experiments on weight loss samples

At the end of weight loss experiments with 150 A/m^2 and 220A/m^2 polarization curves were made using the Bank-MP81 potentiostat. The sweep rate was 20 mV/minute, however a sweep rate of 5 mV/minute was used close to the corrosion potential. The lower sweep rate was needed to obtain an adequate resolution of the measurements. Figure 4.1.8 show the polarization curves produced at the end of the weight loss measurements.

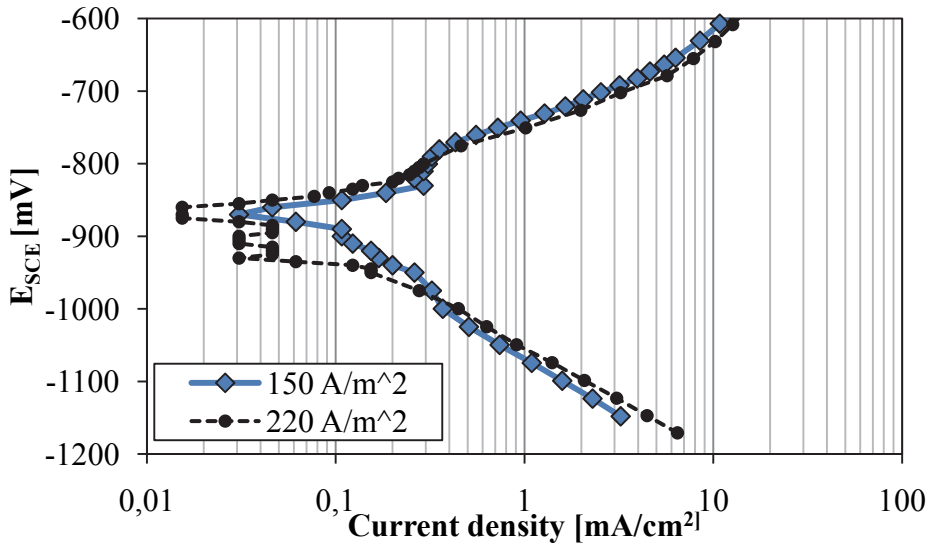

Figure 4.1.8: Polarization curves of samples exposed to 150 A/m^2 and 220 A/m^2 produced at the end of the weight loss experiments.

It is not possible to determine an accurate i_{corr} from the polarization curves, however an indication of the corrosion current density is apparent. By extrapolation of tafel slopes the corrosion current was roughly estimated to 0,04-0,05 mA/m^2. This corrosion current estimation is somewhat higher than the corrosion currents estimated from LPR and weight loss measurements. However considering the uncertainty regarding corrosion current measurements, the results are in adequate accordance with the LPR and WL measurements. The cathodic and anodic tafel slopes estimated from the polarization curve produced at 220 A/m^2 were b_c~150mV/dec and b_a~110mV/dec whilst the polarization curve produced at150 A/m^2 attained b_c~160mV/dec and b_a~95mV/dec. This shows a lowering of the tafel slopes with increasing AC-current density.

Figure 4.1.9 shows the current density response transient after polarization of the WE ±10mV. Without induced AC no instantaneous current rise is observed. When the sample is exposed to AC an immediate elevation of the current density is observed followed by a rapid decrease and stabilization of the current density. This instantaneous current rise increased with increasing AC-current density.

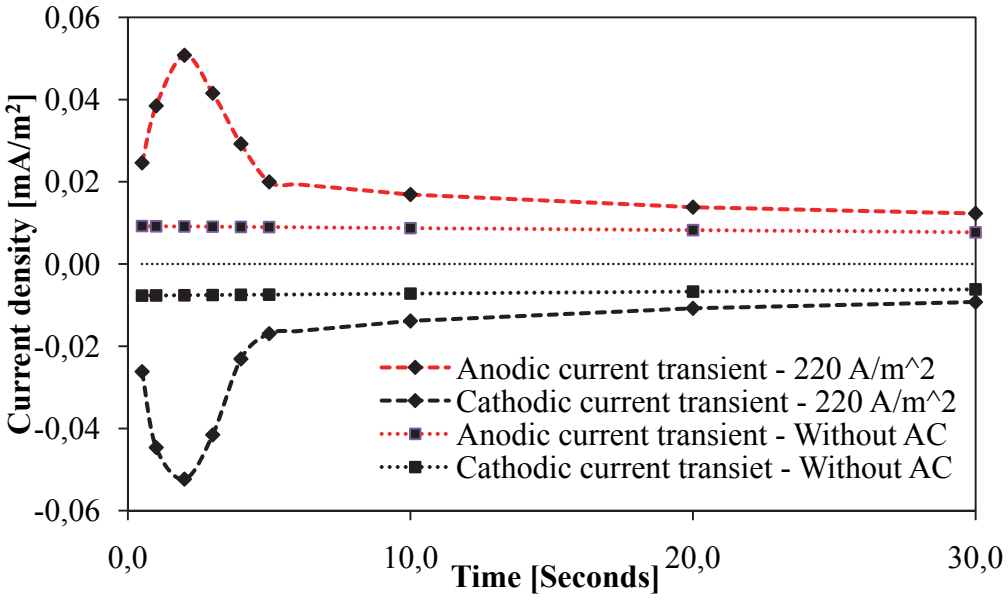

Figure 4.1.9: Current density response after imposing ±10mV during the LPR measurements of samples without AC and when exposed to 220 A/m^2.

4.2 Electrochemical behavior

The objective of the experiments was to elucidate electrochemical effects of an induced AC-current in carbon steel. Deviations from the electrochemical behavior of the steel without AC-current seemed ubiquitous for all experiments exposed to AC-current. Polarization curves were produced at AC-current densities of 0, 100, 150, 220 and 500 A/m^2 respectively. The polarization curves were made using a Pine rotating electrode setup. Rotational speeds of 175 and 350 revolutions per minute (RPM) were selected to attain turbulent flow. This enabled the possibility of observing limiting current of oxygen reduction (i_{lim}) in the polarization curves. Two separate experiments were run on each AC-current density and rotational speed control the reproducibility of the polarization sweep measurements. All dotted lines in the presented graphs are intended to "connect" separate data points for more easy readings. They are not representative for any values between the measurement data points. The signal interference occurring in Figure 4.2.2 in the second parallel at 100 A/m^2 and 500 A/m^2 was caused by a bad wire.

From the polarization curves a decreasing influence of oxygen reduction is observed with increasing AC-current densities. The potential range, in which i_{lim} appeared, decreased with increasing AC-current densities. A particular case was at an induced AC-current density of 150 A/m^2 were the effect of oxygen reduction appeared negligibly small for both rotational speeds. This also appears in the second parallel at 175 RPM and an AC-current density of 220 A/m^2. However this result was not reproducible.

In general, a lowering of the corrosion potential occurred when an AC-current was induced in the steel. From the polarization curves in Figures 4.2.1-2 a relation between corrosion potential and extensiveness of oxygen reduction is apparent. The samples not exposed to AC-currents have a large potential range with limiting current of oxygen reduction and a fairly anodic corrosion potential (~450 mV_{SCE}). Generally at AC-current densities of 100, 220 and 500 A/m^2, the potential range of i_{lim} decrease and the corrosion potentials get more cathodic with increasing AC-current densities. At 150 A/m^2, for both rotational speeds, no significant oxygen reduction reaction is observed. The corrosion potential is approximately 850 mV_{SCE}, which is between 200-400 mV more cathodic compared to the remainder.

Despite this decrease in potential range were limiting current of oxygen reduction occurred, no significant change in limiting current density was observed between the different AC-current densities. Consequently making the estimated corrosion current densities, showed in Figure 4.2.3, almost unchanged with increasing AC-current densities.

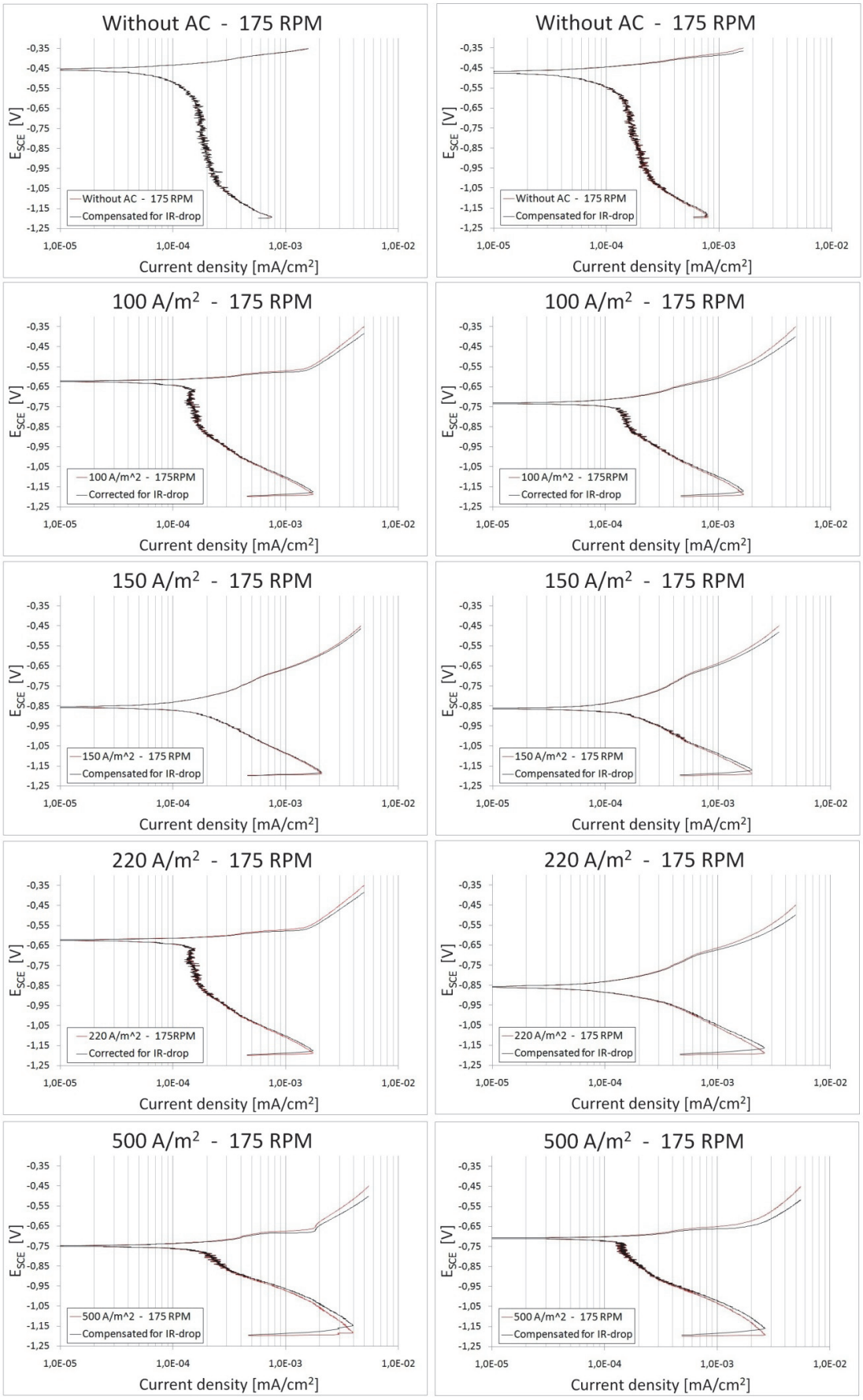

Table 4.2.1: Parallel 1 (left) and parallel 2 (right) of the polarization curves at 175 RPM

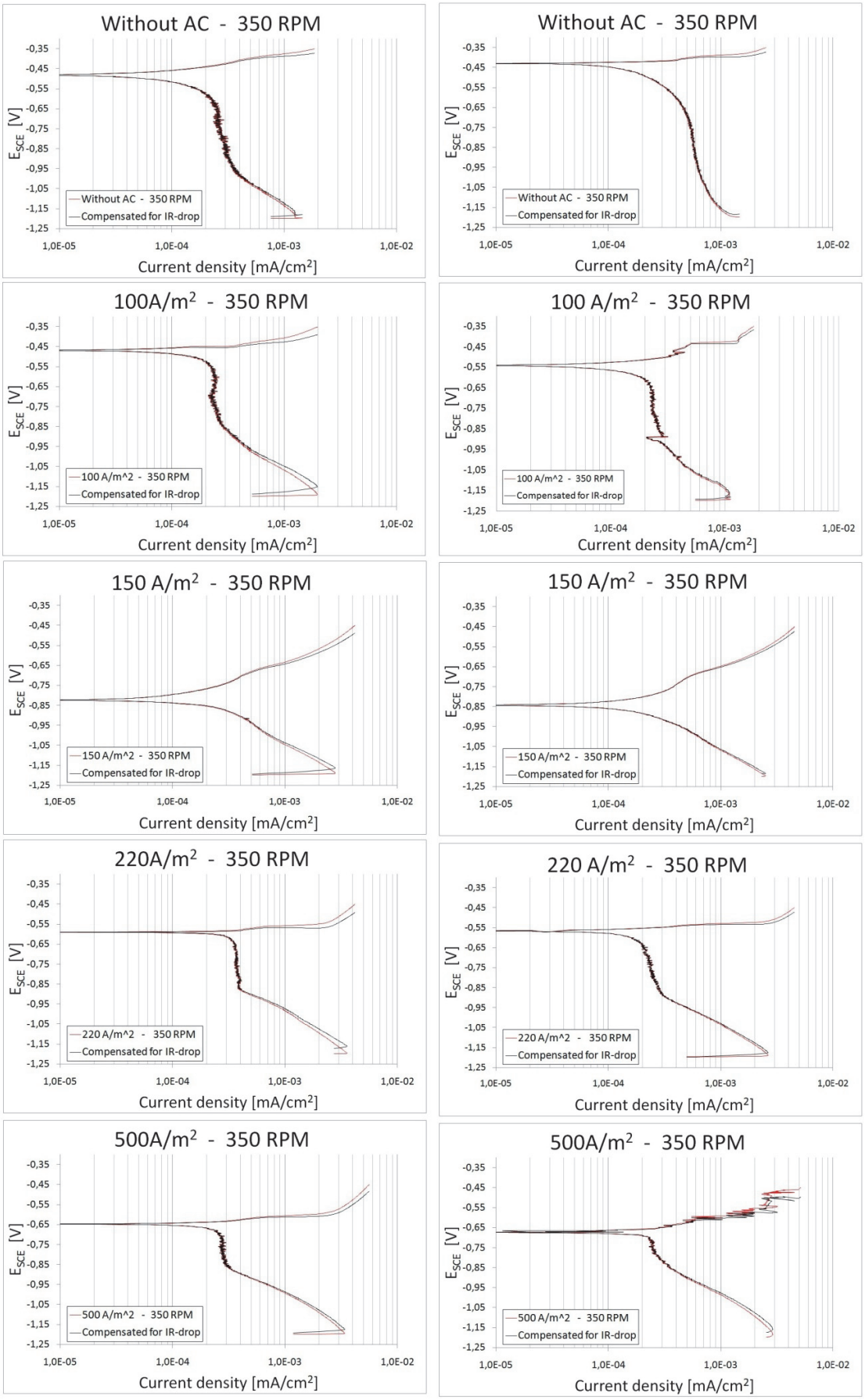

Figure 4.2.2: Parallel 1 (left) and parallel 2 (right) of the polarization curves at 350 RPM.

The corrosion current densities were estimated by finding the intersection between the horizontal line from E_{corr} and the extrapolated cathodic tafel slope (for 150 A/m^2) or the slope of the limiting current density for the remaining AC-current densities.

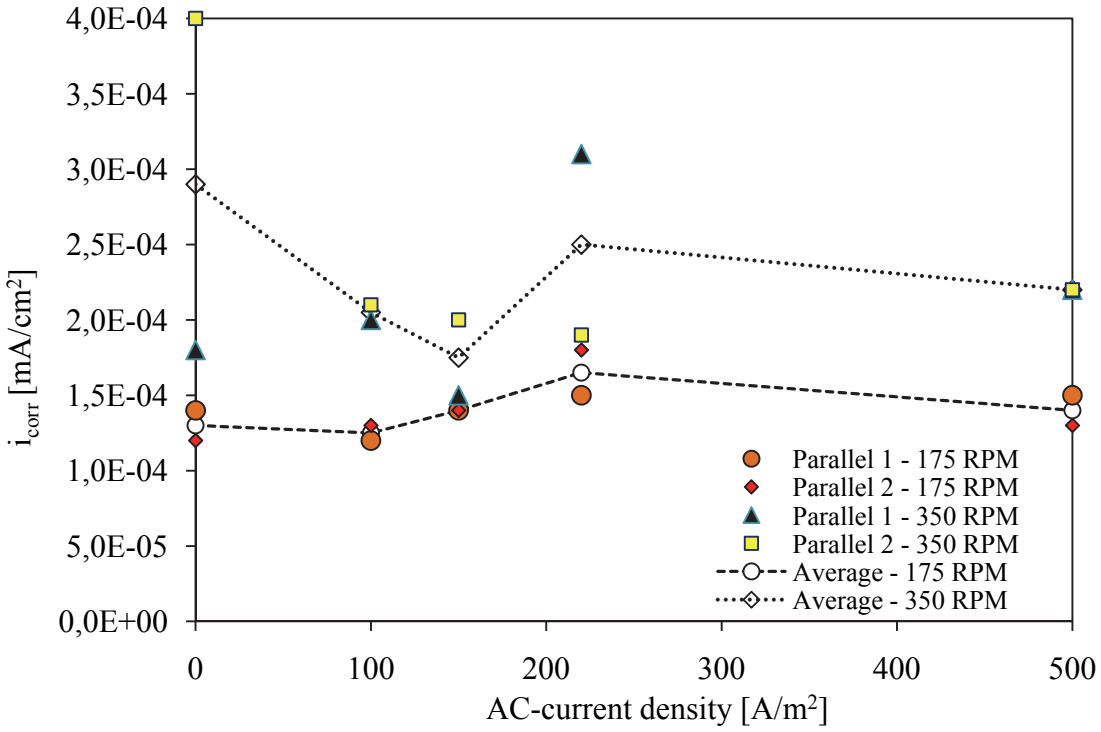

Figure 4.2.3: Estimated corrosion currents at various AC-current densities and rotational speeds.

The cathodic tafel lines got more apparent and showed a decreasing tafel slope with increasing AC-current densities. Anodic tafel slopes are considered "absent" due to pitting above the corrosion potential. At AC-current densities of 150 A/m^2, 220 A/m^2 and 500 A/m^2 a vigorous hydrogen evolution was observed at cathodic DC potentials. In parallel 2 at 175 RPM and AC-current densities of 0 A/m^2 and 100 A/m^2 it was impossible to determine the respective cathodic tafel slopes. The former due to the lack of tafel behavior, and the latter due to signal interference.

Figure 4.2.4 shows the cathodic tafel slopes at the different rotational speeds and AC-current densities. The trend line is an average of the slopes at intended to represent a picture of the general cathodic tafel development at the different AC-current densities. The steepest tafel slope appears on the measurements without induced AC. At 100 A/m^2,

150 A/m^2 and 220 A/m^2 the tafel curves have a somewhat lower slope. However there is no significant alteration in the cathodic tafel slopes between the different parallels at these AC-current densities. At 500 A/m^2 the lowering of the tafel slopes is more apparent.

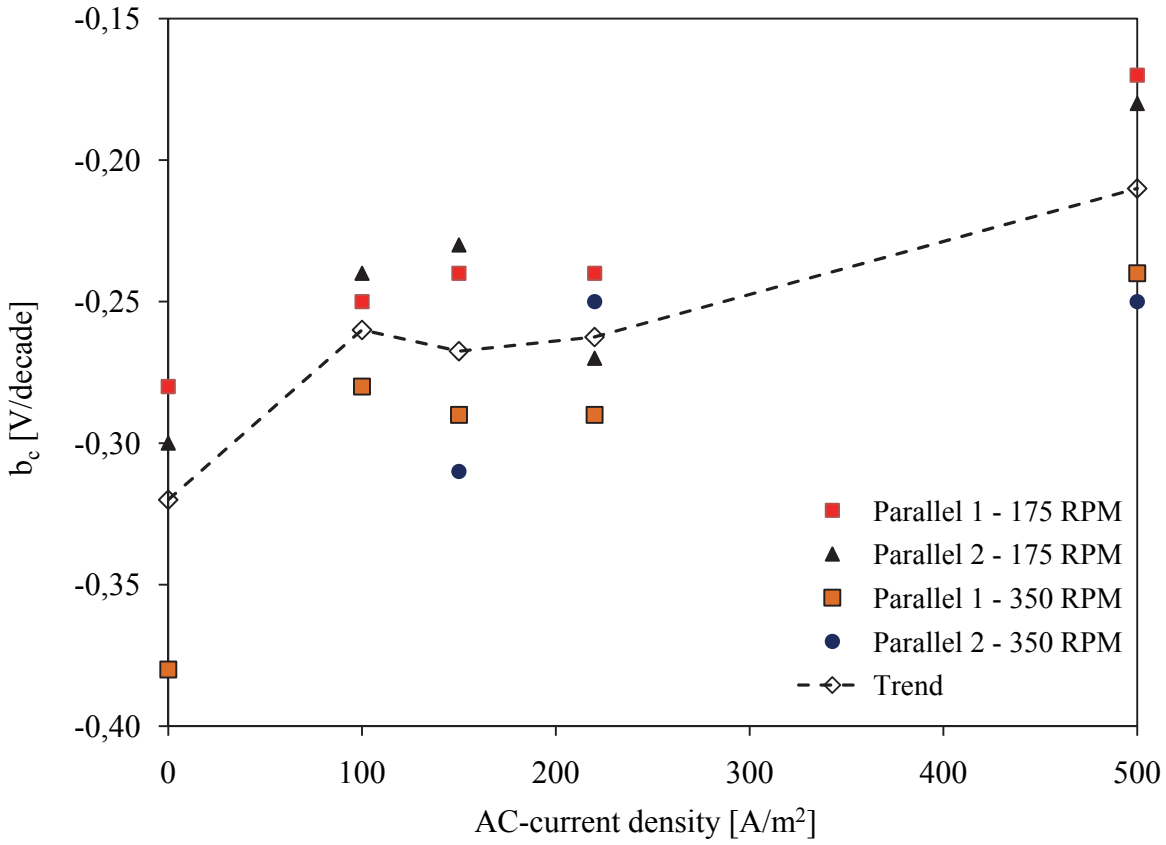

Figure 4.2.4: Cathodic tafel slopes at various AC-current densities and rotational speeds.

Oscilloscope measurements

From the oscilloscope phase displacements between the alternating cell voltage and AC-current was calculated. The distances between the voltage and current amplitudes were measured from snapshots captured at the beginning and the end of the polarization experiments. For rotational speeds of 175 RPM the measured phase displacements were 10,3° at 100 A/m^2 and 5,1° for 150-, 220- and 500 A/m^2. By mistake snapshots were not captured at AC-current densities of 220- and 500 A/m^2 at 350 RPM, however the phase displacements for 100 A/m^2 was 10,1° and 5,1° for 150 A/m^2.

4.3 Surface morphology

The weight loss samples were investigated in SEM captured in the SEM after the weight loss experiments to observe the nature of the corrosion products and if pitting occurred. Notice that not all picture series are captured at the same magnifications. By mistake pictures of the sample exposed to 50 A/m2 were not captured.

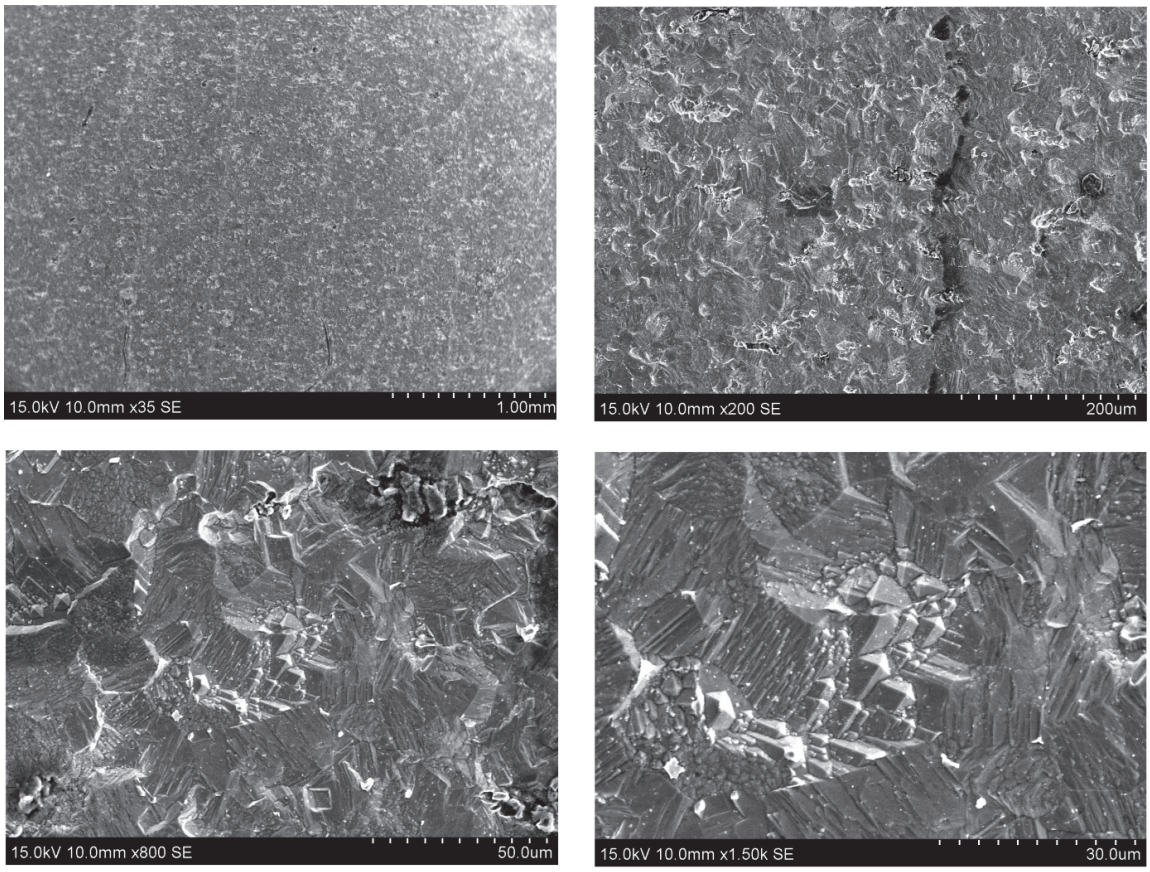

Figure 4.3.1: SEM pictures of the sample without induced AC prior to removal of corrosion products.

In the weight loss experiments without induced AC, showed in figure 4.3.1, the oxide layer was dense and no pits were observed. The oxide formation seemed to grow in preffered directions. The oxides appeared to grow in a columnar manner and attain a pyramidal shape.

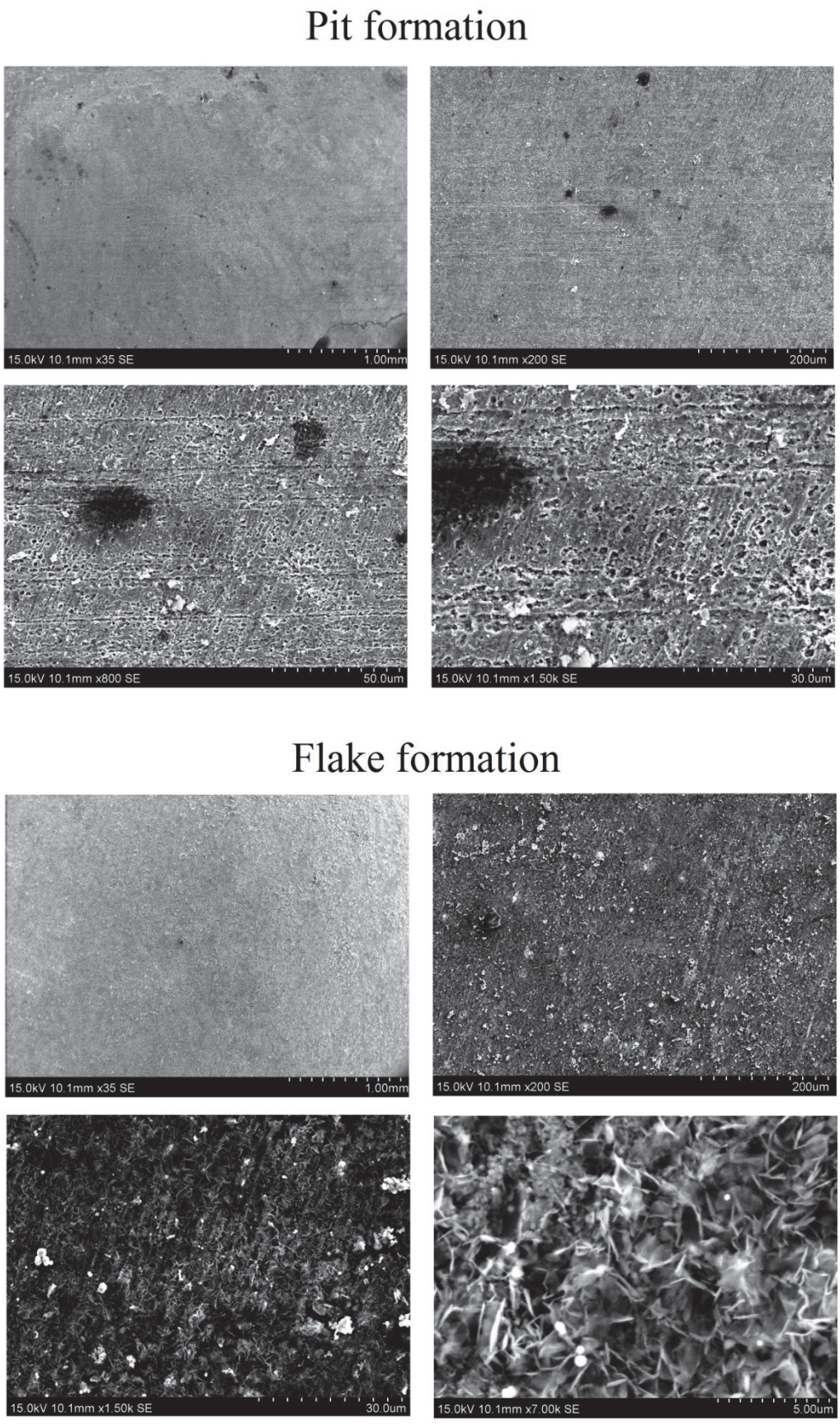

Figure 4.3.2: At 75 A/m^2 the sample experienced pitting/porous oxide layer (top picture) and flake oxide formation (bottom picture).

Figure 4.3.2 show sample exposed to 75 A/m^2 before removal of the corrosion products. Two regimes of corrosion behavior appeared at this AC-current density. The top picture shows oxide and pitting behavior. The bottom picture shows the formation of a flake-oxide.

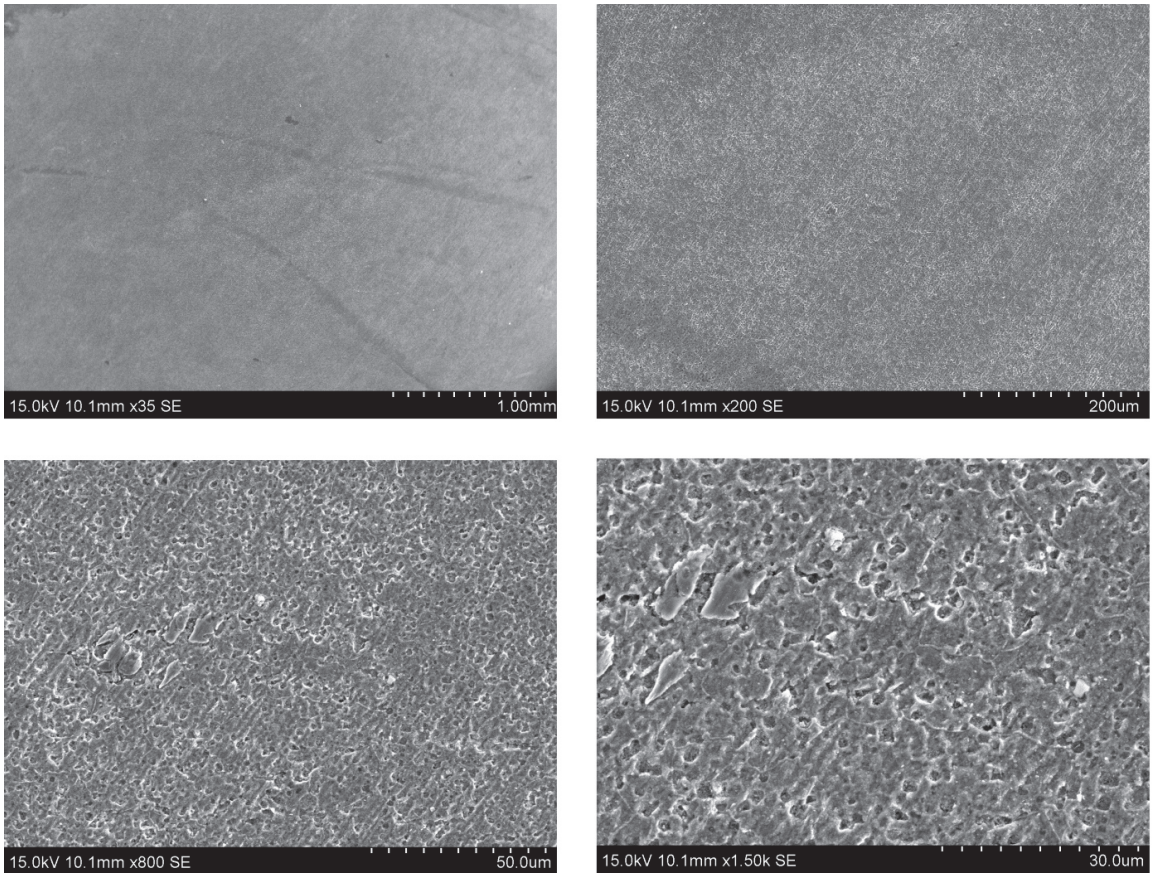

Figure 4.3.3: Pitting or formation of a porous oxide layer at 100 A/m^2 prior to removal of the corrosion products.

From Figure 4.3.3 the formation of pits in combination with an oxide layer is apparent on the sample exposed to 100 A/m^2 before removal of the corrosion products. The pits were evenly distributed on the entire exposure area. Typical size of the pits was between 2-5 μm in diameter.

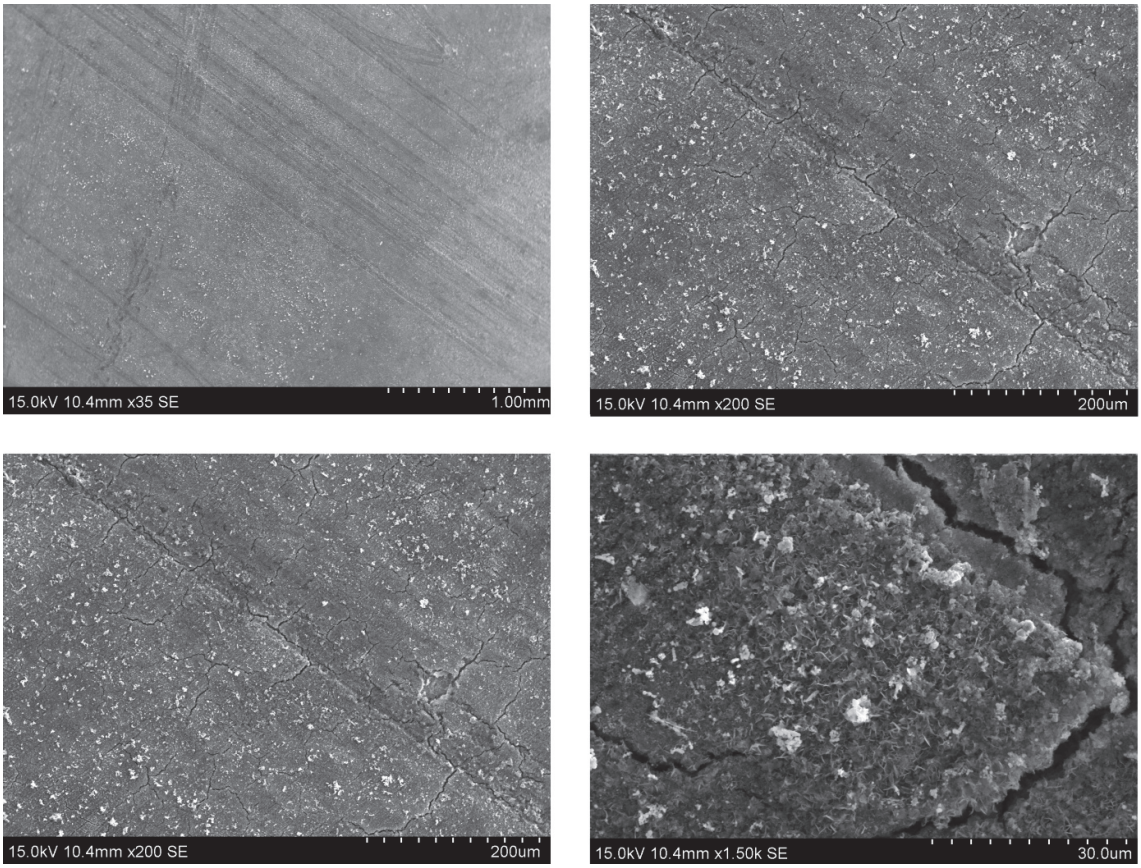

Figure 4.3.4: Formation of a brittle "flake" oxide on the steel sample at 150 A/m^2. Picture is captured prior to the removal of corrosion products.

Figure 4.3.4 displays the weight loss sample exposed to an AC-current density of 150 a/m^2 obtained a brittle oxide layer with a flaky surface appearance. However the cracks are probably introduced mechanically after the experiment. At a magnification of 1500X the oxide shows flakes similar to the ones observed at 75 A/m^2. This type of oxide represented the entire sample surface area.

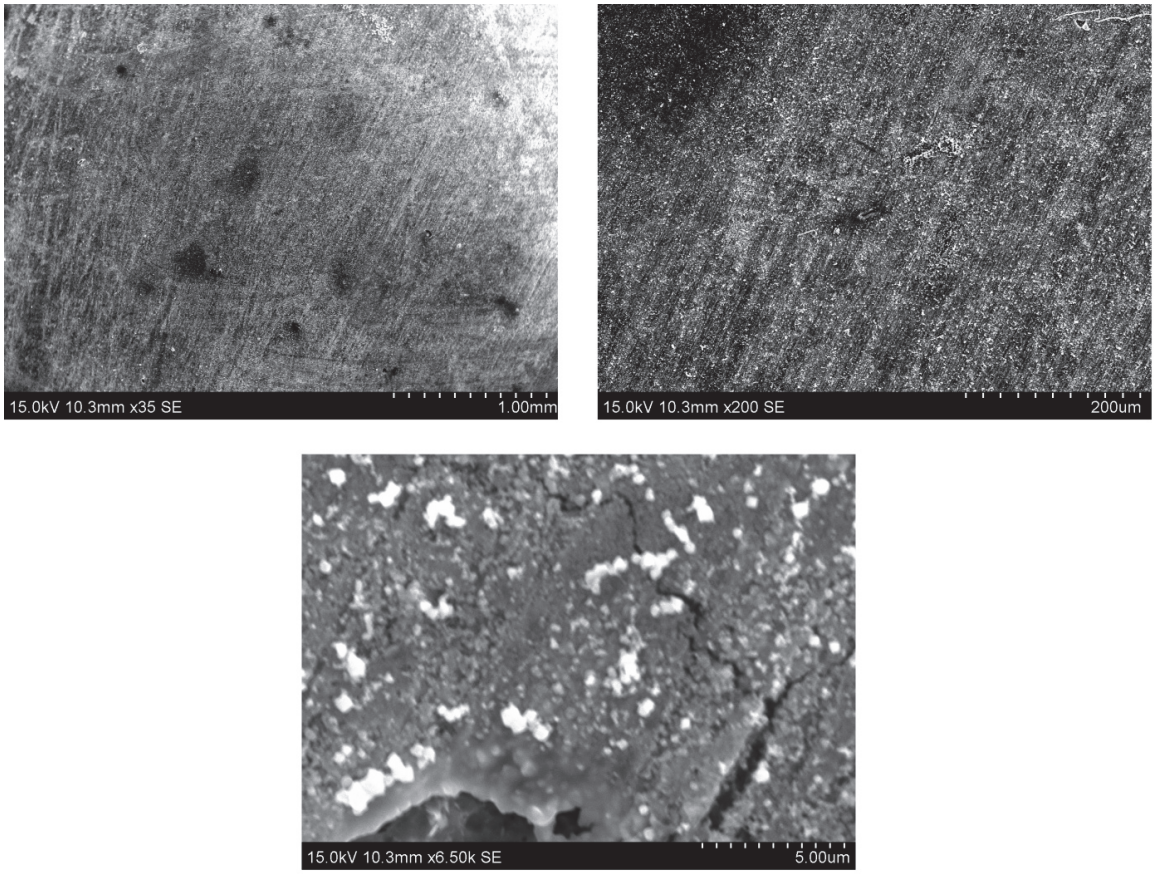

Figure 4.3.5: Formation of a brittle oxide on the steel sample at 220 A/m^2. Picture is captured prior to the removal of corrosion products.

Figure 4.3.2 shows pictures of the sample exposed 220 A/m^2 captured in the SEM at various magnifications. A brittle oxide layer similar to the one found at 150 A/m^2 was observed on the entire surface of the sample exposed to 220 A/m^2. However no signs of flake formation were found. The white particles may be salt remains.

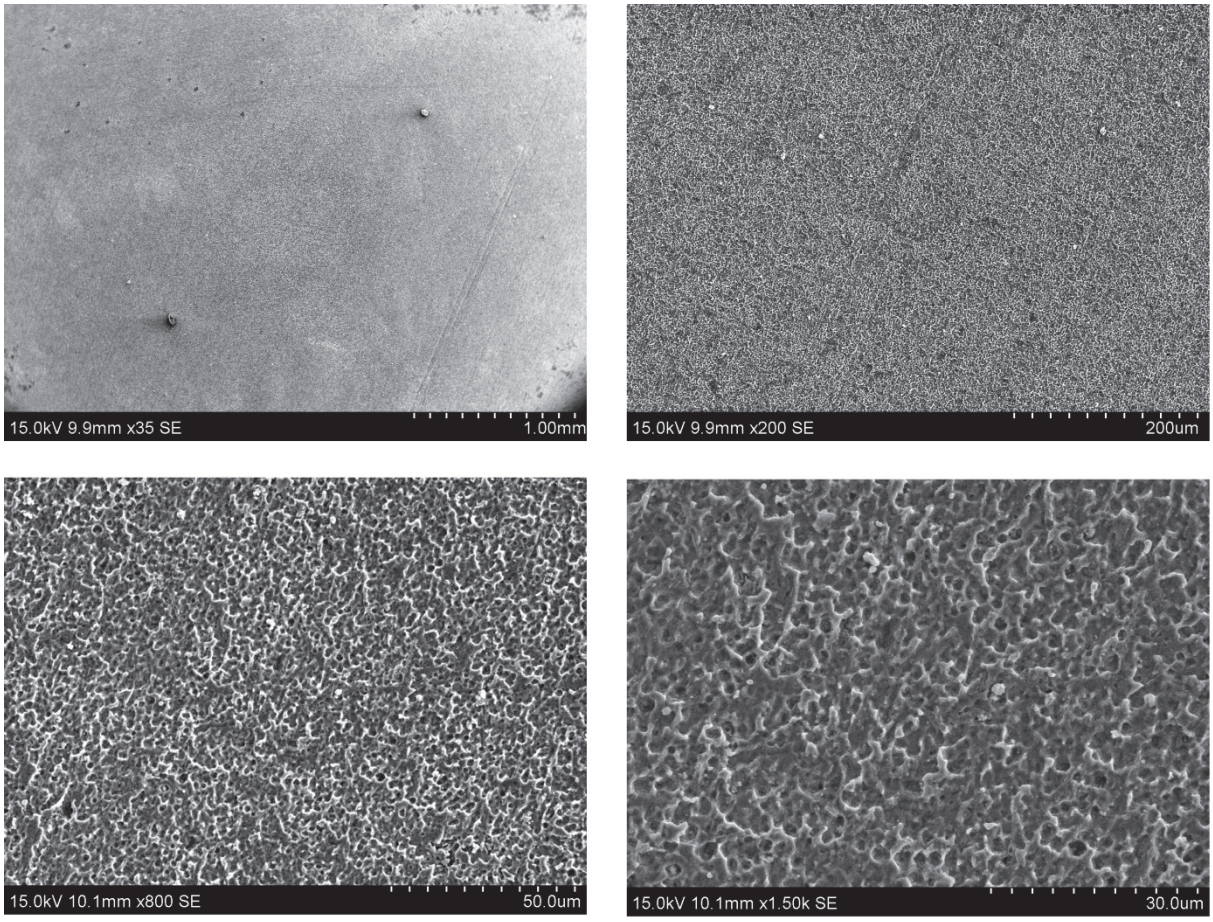

Figure 4.3.6: Porous oxide formation and/or pitting behavior for sample exposed to 500 A/m^2.

Figure 4.3.6 shows the sample exposed to 500 A/m^2 at various magnifications. The entire surface showed signs of pitting behavior or the formation of a porous oxide layer. The pits are evenly distributed and have diameter diameters varying between ~ 2-5µm.

The following pictures in figures 4.3.7-12 are captured in the SEM after the corrosion product removal procedure.

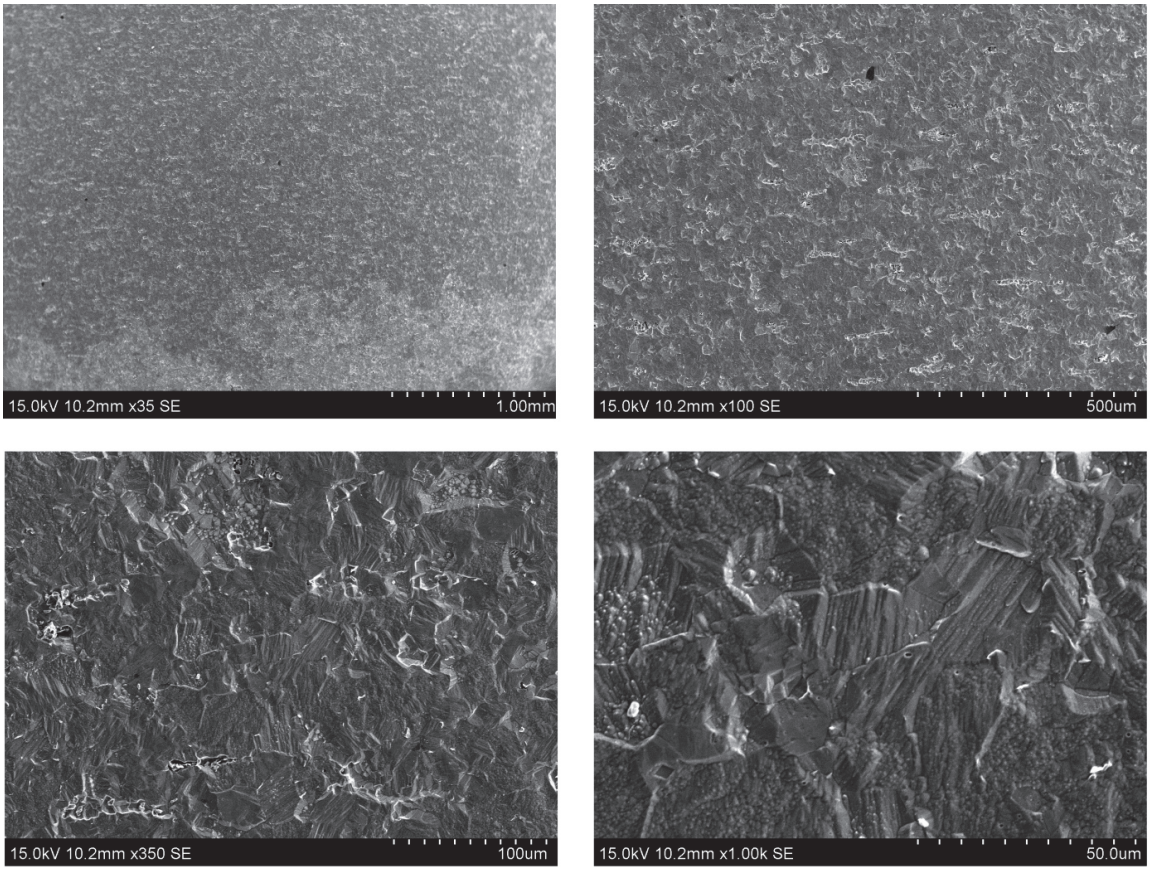

Figure 4.3.7: SEM images of sample without AC after the procedure for removal of corrosion products.

Figure 4.3.7 displays SEM pictures captured after the procedure for removal of corrosion products. The surface showed no signs of pitting and uniform corrosion is the dominating corrosion process. Unexpectedly some of the corrosion products appeared to remain after the procedure for corrosion product removal.

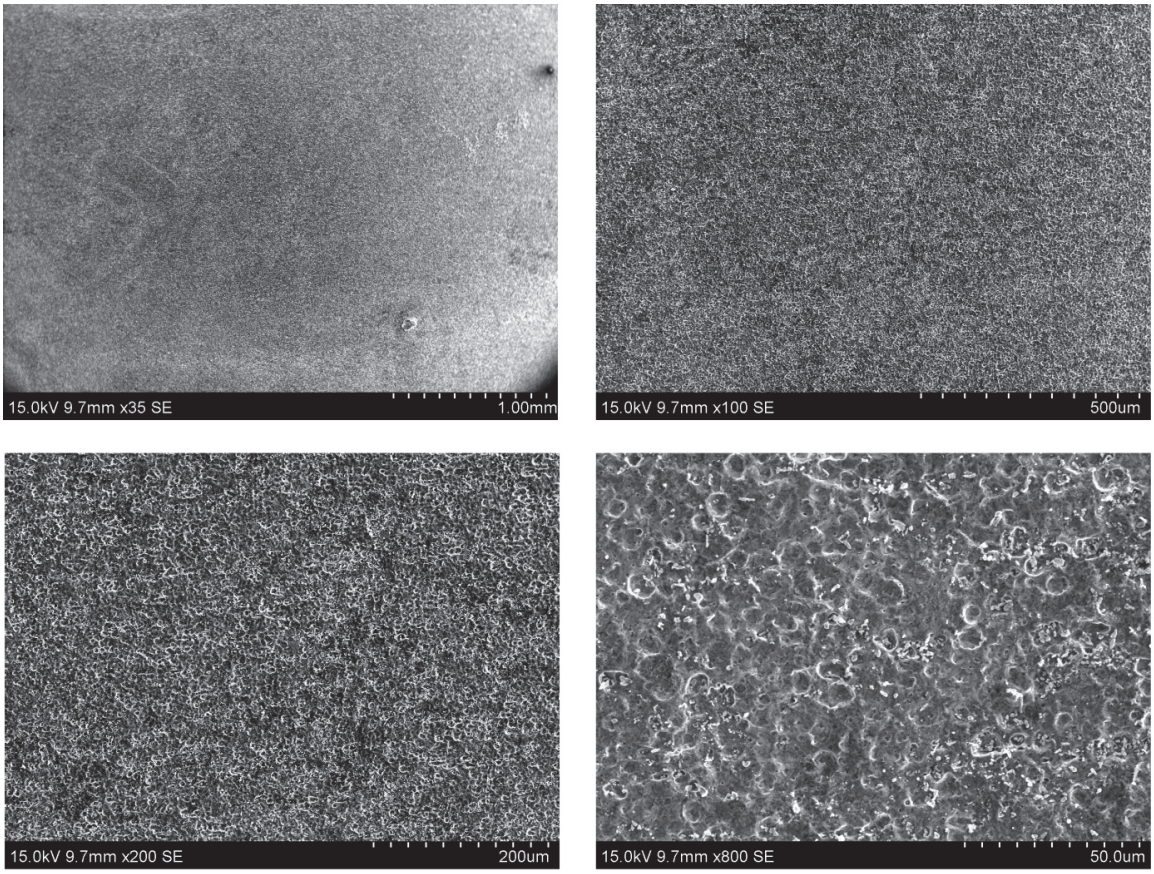

Figure 4.3.8: SEM pictures of sample at 75 A/m^2 captured after removal of corrosion products.

Figure 4.3.8 displays the sample exposed to 75 A/m^2 at various magnifications. Pitting is the dominating corrosion form for the entire exposure area, and the pits are evenly distributed. The pit diameter varies between approximately 5-10µm, however a large number of what appears to be small pits (~1µm) is observed.

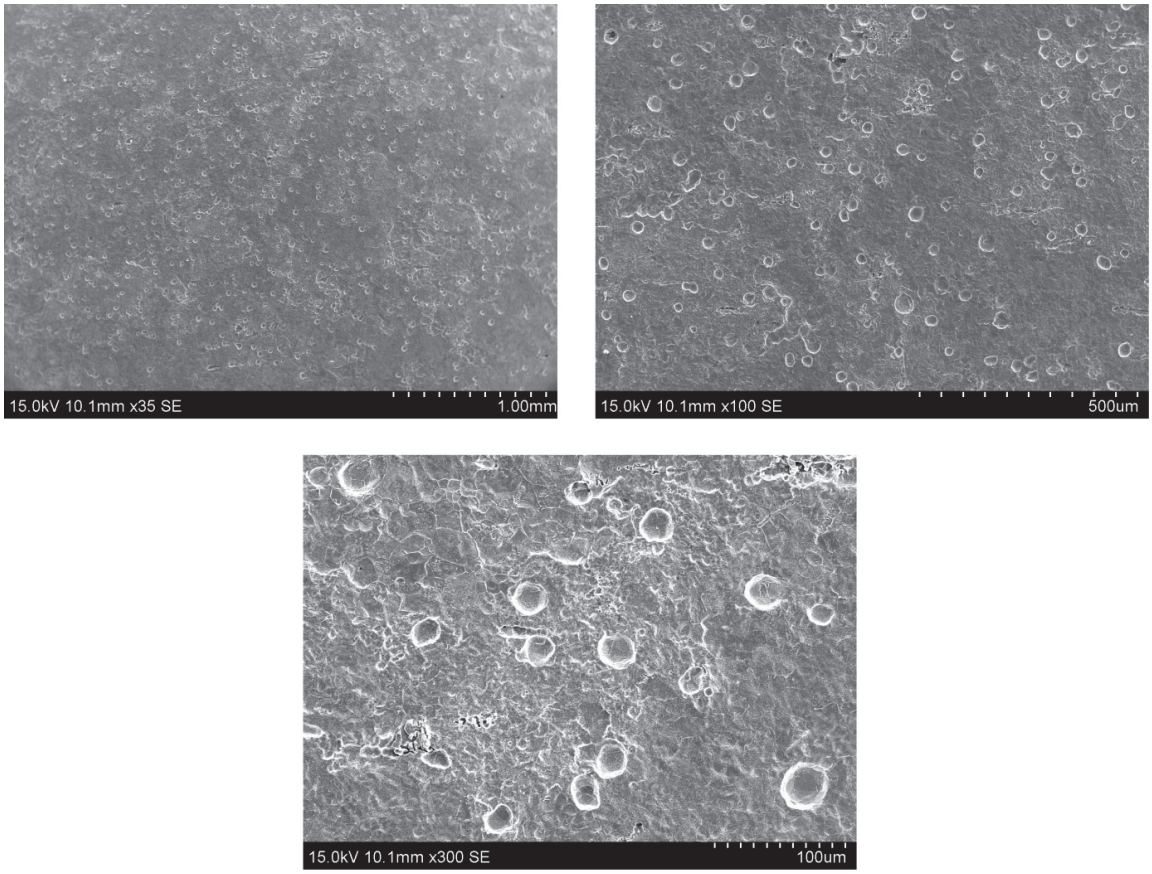

Figure 4.3.9: SEM pictures captured of sample exposed to 100 A/m^2 after removal of corrosion products.

The sample exposed to 100 A/m^2 gained the largest pits of all the AC-current densities. Pits with a diameter varying between 20-50µm was evenly distributed over the entire exposure area. However the pit density was smaller compared to the other samples experiencing pitting corrosion.

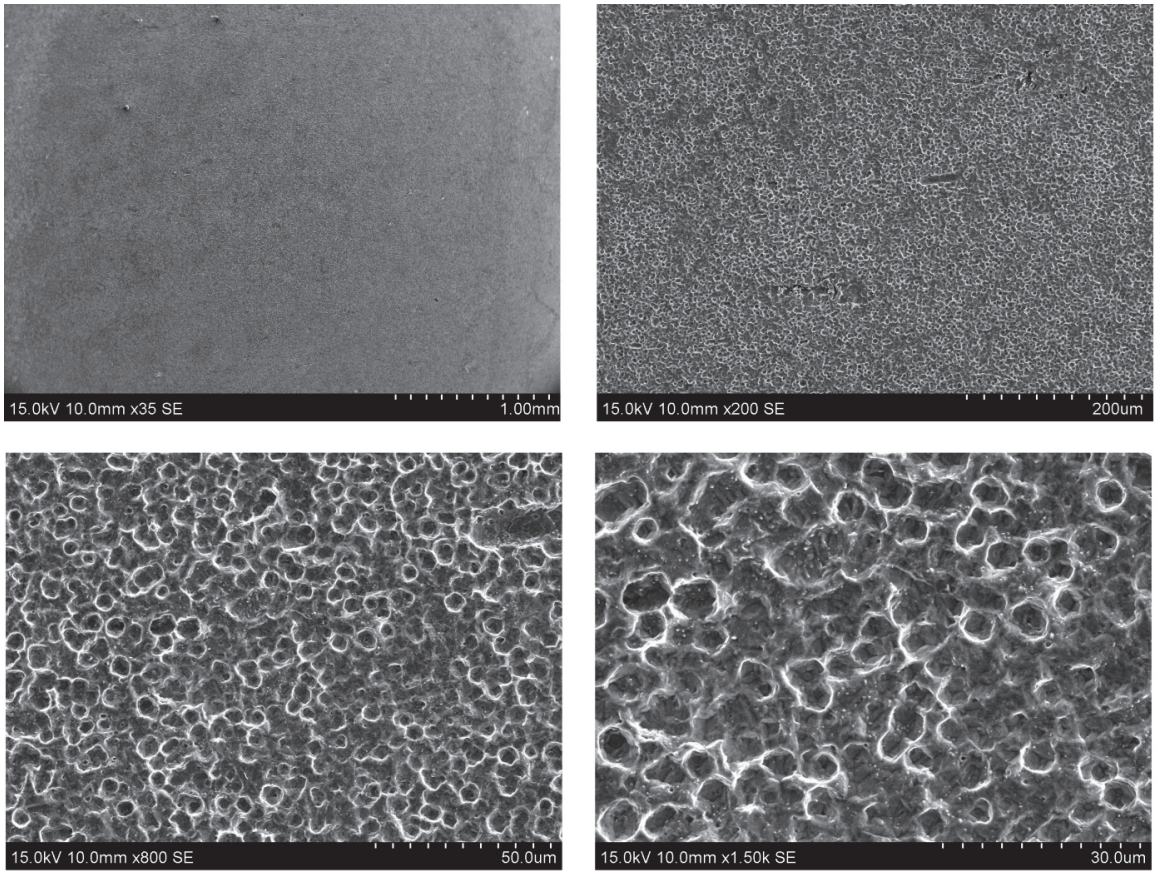

Figure 4.3.10: SEM pictures captured of sample exposed to 150 A/m^2 after removal of corrosion products.

Figure 4.3.10 shows picures of the sample exposed to 150 A/m^2 after the removal of corrosion products. This AC-current represents the largest pit density. Pit sizes varied between ~ 3-6µm. The pits were evenly distributed troughout the entire exposure area.

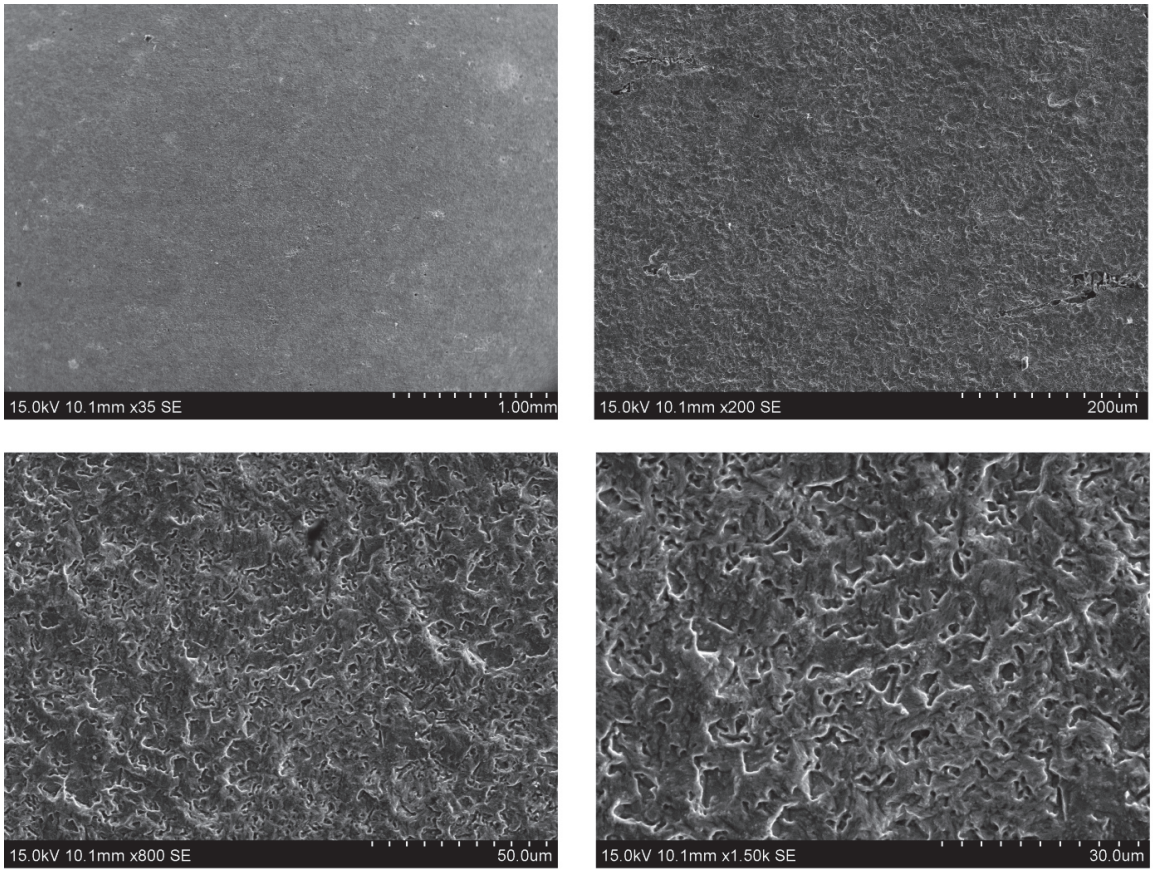

Figure 4.3.11: SEM pictures captured of sample exposed to 220 A/m^2 after removal of corrosion products.

The sample exposed to 220 A/m^2, showed in Figure 4.3.11 experienced pitting formation of an acicular character. A very high pitting density is observed. The pits are evenly distributed over the entire exposure area.

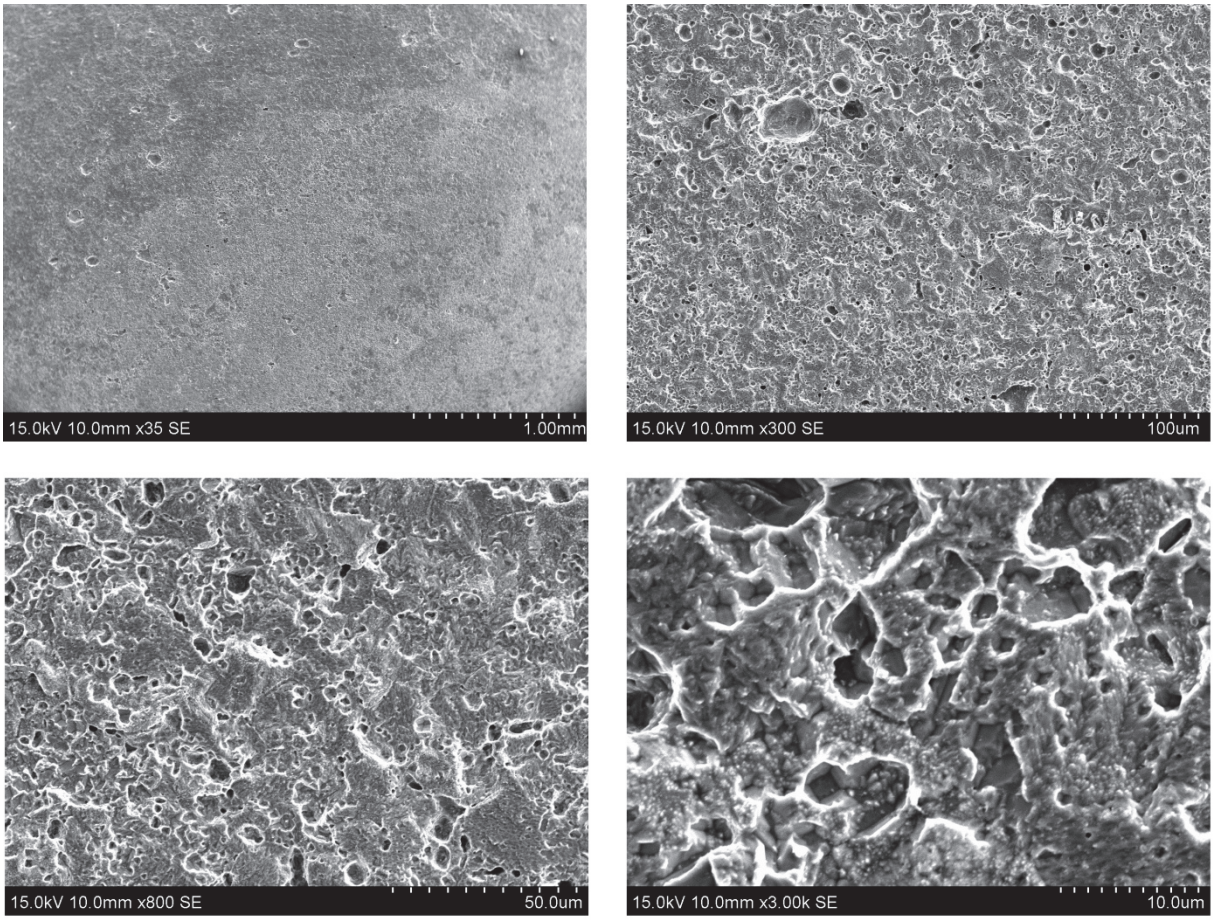

Figure 4.3.12: SEM pictures captured of sample exposed to 500 A/m^2 after removal of corrosion products.

The sample exposed to 500 A/m^2 showed in Figure 4.3.12 experienced pitting. The pit sizes varied in shape and size but in the pits attained in general a non-circular shape with straight edges. Typical sizes of the pits varied between ~ 3-10µm in diameter. The pits were evenly distributed over the entire exposure area.

5. Discussion

5.1. Corrosion testing

The corrosion rates for samples exposed to AC-current densities below 500 A/m^2 show no clear indication of an increase in corrosion rates. The weight loss experiments at 500 A/m^2 both samples showed an increase in corrosion rate compared to the experiments without AC.

For AC-current densities of 100 A/m^2 to 220 A/m^2 the measured corrosion rates appear slightly higher than for the experiments with lower AC-current densities and without AC. At 50- and 75 A/m^2 the measured corrosion rates were in fact lower than the corrosion rates without induced AC. However it is worth mentioning that the samples exposed to 50- and 75 A/m^2 was exposed to insignificant amounts of corrosion outside the intended exposure area compared to the remainder. The sample exposed to 75 A/m^2 is shown in Figure 4.1.4 were no significant corrosion outside the intended exposure area was observed. This probably made the weight loss lesser than for the remaining samples. All other samples experienced corrosion outside the immersion area. It is difficult to determine the severerity of the additional corrosion attacks, however the attacks appeared to be of the same magnitudes. These additional corrosion attacks make the corrosion rate measurements less reliable.

Linear polarization resistance measurements.

From the linear polarization measurements no achange in corrosion current occurred at the different AC-current densities. The constant B from the Stern-Geary equation decreased with increasing AC-current densities. This is explained by the lowering of anodic and cathodic tafel slopes with increasing AC-current densities. The polarization resistance Rp' also showed a decreasing trend with increasing AC-current densities. This is explained by the increase in current response (from LPR measurements) with increasing AC-current densities. To attain valid estimations of the R_p values, the potential drop of 9,3Ω introduced by the inductance was subtraced from the total resistance in the circuit. The corrosion current estimated from the LPR measurements remained unaltered regardless of the AC-current density. This is explained by the simultaneous lowering of both B and R_p', which in turn results in an unaltered corrosion current.

5.2 Electrochemical testing

Bosch (1998) reported that corrosion rates under mixed control based on polarization curves are limited by limiting current of oxygen reduction.[13] This is in accordance with the polarization curves produced in the rotating electrode experiments in this thesis. The reported polarization curves suggested tafel behavior with no AC and low AC-current densities, and furthermore an increasing effect of diffusion controlled limiting current with increasing AC-current densities. This contradicts the observations in this work which moreover imply the opposite behavior. For the polarization experiments, the largest area in which i_{lim} occur appear without AC and the effect of limiting current of oxygen reduction seem to decrease with increasing AC-current densities. A particular case arose at 150 A/m^2 were little, or no effect of oxygen reduction was observed. Bosch (1998) also suggests lowering of the corrosion potentials with increasing AC. This trend is also observed in the polarization curves produced from the rotating electrode setup. However the decrease in corrosion potential seems to be more dependent on the limiting current of oxygen reduction than of AC-current density. Experiments exposed to 150 A/m^2 attained the most cathodic corrosion potentials and had correspondingly the lowest "amount" of oxygen reduction. A suggested relation between AC-current density and corrosion potentials may be the influence of AC-current on the extent of oxygen reduction.

Oxide formation

A significant alteration of the oxide formation for samples exposed to AC compared to samples without AC was observed. All the samples exposed to AC attained a dark oxide layer visible with the naked eye. This oxide film got darker with increasing AC-current density. The sample investigated without induced AC gained a oxide layer which seemed to grow in preffered directions and attained columnar and/or pyramidal shapes. For the samples exposed to induced AC-current densities of 75 A/m^2, 100 A/m^2 and 500 A/m^2 the oxide layer appeared to undergo local attacks of the oxide layer causing pits in the oxide layer to develop. The samples exposed to 150 A/m^2 and 220 A/m^2 attained an oxide layer with several cracks. At 150 A/m^2 and partially at 75 A/m^2 a flake-shaped oxide was observed. However it is difficult to determine whether this flake oxide was formed during the experiments or after.

Surface after removal of oxide layer

All samples exposed to AC-current experienced corrosion attacks of a local character. Sample without AC-current attained a uniform corrosion attack. However the etching rate of different grains seems to differ due to the combination of a smooth corroded surface combined with a more striated appearance. For the samples exposed to AC-current the formation of pits (of varying in shape and size) seems ubiquitous. At 75 A/m^2 and 150

A/m^2 the pit sizes varied between approximately 3-10µm. The largest pits were observed at an AC-current density of 100 A/m^2. At 220 A/m^2 the pits attained in general a more oblong shape compared to the lower AC-current densities. The oblong pits appear to follow grain boundaries. This may imply a facilitation of grain boundary corrosion at high AC-current densities. At 500 A/m^2 the pits appear to take shape of the grain boundaries. From the weight loss measurements a slight increase in corrosion rate was measured at this AC-current density. However the LPR measurements showed no increase in the estimated corrosion current density. Hence a possible "mechanical" corrosion attack may be suggested. As mentioned, at 220 A/m^2 pits was observed to form preferably along grain boundaries and at 500 A/m^2 the pits appeared to take the shape of grains. This may indicate an increasing grain boundary corrosion mechanism at high AC-current densities resulting in the "loss" of grains due to the grain boundary corrosion. This is a non-faradaic corrosion contribution and hence not able to measure using electrochemical testing such as LPR and polarization curves. Another observation is the appearance of particles with the shape of nitrides inside pits on sample exposed to 500 A/m^2 after the procedure for oxide layer removal. This is however unexpected due to a very low N-content in the steel. If the particles were to be nitrides the formation of local galvanic cells and selective dissolution is possible.

5.3 Further work

Experimental procedure development

The sources of error related to the experimental work carried out during this thesis are discussed as a part of the development of the experimental setups and procedures.

Sample preparations

Due to the additional corrosion attacks of the weight loss samples, an improved sample preparation procedure is needed. There are two obvious alternatives. The first is to grind the entire sample (not only the immersion area) to a 1000 grit finish prior to the experiments. Figure 4.1.4 shows a sample in which the entire sample were grinded. The sample showed no significant signs of corrosion attacks outside the intended immersion area. The second sample preparation procedure involves painting of the entire sample area except the immersion area using a carbon steel wire to attain electrical conductivity. Figure 5.3.1 shows the suggested method for avoiding unwanted corrosion.

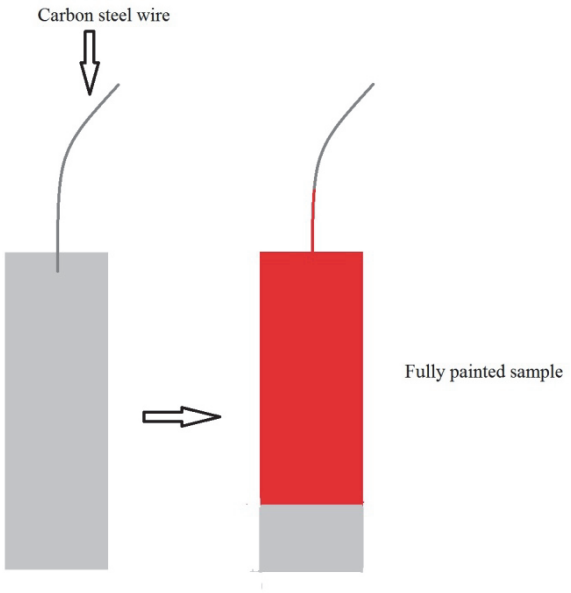

Figure 5.3.1: Proposed sample preparation were the entire sample area except the intended exposure area is painted.

In addition the steel should be more comprehensively examined by determining the microstructure using a light microscope. Knowledge about the microstructure may contribute to understanding the different oxide formations and corrosion attacks.

Weight loss experiments parallels should be performed with the suggested improvements of the experimental procedure. Additional weight loss experiments should be performed with LPR measurements each day of immersion. Another parallel of weight loss experiments should be carried out including everyday LPR measurements and polarization sweeps at the end of the experiment.

Corrosion testing improvements

Weight loss experiments comparing AC-current density versus AV peak by using samples with different exposure area resulting in the same current density but different AV peaks. It is also desirable to measure and log the reference potential on both sides of the inductance to observe the difference in polarization curves and LPR measurements. Weight loss experiments with induced AC-current in the steel sample should be carried out in combination with an aluminium sacrificial anode. Comparing the DC-current supply from the sacrificial at various AC-current densities and comparing them to a setup with no induced AC, should give an impression of the increased anode mass usage. Weight loss measurements from the exposed steel sample (and sacrificial anodes if possible) should be performed. This facilitates estimation of anode consumption at various AC-current densities and the corresponding weight loss of the cathodically protected steel. Polarization curves at various AC-current densities should also be performed for aluminium. The anodic part of the aluminium polarization curve and the cathodic part of the polarization curve of the steel should be plotted in the same curve determining i_{couple}. This should be compared to the weight loss experiments using a sacrificial aluminium anodes to see whether the polarization curves give similar results.

X-ray diffraction or microprobe analysis should also be performed to investigate the oxide layers at the various AC-current densities. Glow discharge optical emission spectroscopy should also be carried out determining chemical composition and depth profile of the oxide layers at different AC-current densities. Further investigation of the oxide formations and sample surfaces at the different AC –current densities in the SEM including EDS-analysis should be performed.

Local pH levels (adjacent to the sample surface) and bulk solution pH prior to and after both polarization- and weight loss experiments at various AC current densities should be carried out to investigate the possibility of alkalization. This should be performed both with and without cathodic polarization of the steel.

6. Conclusions

Corrosion testing

Weight loss experiments show that all tested AC-current densities below 500 A/m^2 show no clear increase in corrosion current densities and they are in an approximate accordance with the i_{corr} measurements from the LPR measurements. This implies satisfactory corrosion rate measurements from the LPR measurements. At 500 A/m^2 the measured corrosion rate and corresponding i_{corr} was slightly higher than for the remaining AC-current densities. This may imply a lower credibility of the estimated corrosion currents from the LPR measurements at high AC-current densities. The corrosion current densities estimated from the LPR measurements remained unaltered at all AC-current densities.

The two polarization curves at 150- and 220 A/m^2 produced at the end of the weight loss experiments roughly showed a similar corrosion current densities as from the LPR-measurements. The constant B from the Stern-Geary equation estimated from LPR showed a decreasing trend with increasing AC-current densities, and was related to the corresponding lowering of anodic and cathodic tafel slopes. Polarization resistance Rp' also showed a decreasing trend with increasing AC-current densities. This is explained by the increase in current response (from LPR measurements) with increasing AC-current densities.

A suggested corrosion mechanism causing the increase in corrosion rate at 500 A/m^2 is facilitation of grain boundary corrosion resulting in the loss of grains during the weight loss experiments. This is a non-faradaic corrosion contribution which also supports the unaltered corrosion current measurements from the electrochemical testing.

However all weight loss samples exposed to AC-currents showed significant pitting. Conventional corrosion rate calculations based on LPR-measurements and polarization curves are unable to detect pitting formation and may therefore be regarded incapable as a corrosion monitoring method for steels exposed to AC-currents.

Electrochemical testing

From the polarization curves produced by the rotating electrode setup a decrease in potential range in which limiting current appear is observed with increasing AC-current densities. This change in potential range in which i_{lim} occur also appeared to be related to the measured corrosion potentials at the various AC-current densities. A particular case is for the rotating electrode samples exposed to 150 A/m^2 in wich the measurements seem unaffected by i_{lim}. This observation also corresponds to the other with a much lower measured corrosion potential than the remaining AC-current densities. The estimated corrosion current densities from the potential curves are unaffected by AC-current.

A lowering of cathodic tafel slopes is observed with increasing AC-current densities. Anodic tafel slopes are considered absent due to pitting behavior above the corrosion potentials.

Abbreviations

SCE	Saturated Calomel Electrode
AC	Alternating Current, [A]
AV	Alternating Voltage, [V]
DC	Direct current, [A]
f	Frequency, [rad/sek]
V_p	Peak voltage, [V]
E	Potential, [V]
E_{corr}	Free corrosion potential of metal, [V]
F	Faradays constant, [C/ekv]
i	Current density, [A/cm^2]
i_{gr}	Limiting current density, [A/cm^2]
i_f	Faradaic current density, [A/cm^2]
i_{dl}	Double layer capacitance current density, [A/cm^2]
C_{dl}	Double layer capacitance, [µF]
R_s	Resistance in the electrolyte, [Ω]
Z_p	Non-linear polarization impedance, [Ω]
LPR	Linear Polarization Resistance
SEM	Scanning Electron Microscope
EDS	Energy Dispersive Spectroscopy
GD-OES	Glow Discharge Optical Emission Spectroscopy
LV-SEM	Low Vacuum Scanning Electron Microscope

References

1. **Lazzari L., G.S., Ormellese M., Bolzoni F., *Laboratory Test Results of AC Interference on Polarized Steel.* Corrosion 2003, NACE, Houston, Texas, Paper No. 03704, 2003, pp. 1-13., 2003: p. 13.**
2. **Stamnes, I., *AC-korrosjon av rørstål.* Master's Thesis, Norwegian University of Science and Technology (NTNU), Trondheim, 2010.**
3. **Hesjevik, S.M., *Interim Report, AC Corrosion Testing.* 2009, Statoil: Trondheim.**
4. **Goidanich, S., L. Lazzari, and M. Ormellese, *AC corrosion - Part 1: Effects on overpotentials of anodic and cathodic processes.* Corrosion Science, 2010. 52(2): p. 491-497.**
5. **Pagano, M.A. and S.B. Lalvani, *Corrosion of mild steel subjected to alternating voltages in seawater.* Corrosion Science, 1994. 36(1): p. 127-140.**
6. **Gummow, R.A., Wakelin, R.G., Segall, S.M., *AC Corrosion - A New Challenge to Pipeline Integrity.* Corrosion 98, NACE, Houston, Texas, Paper No. 566, 1998, pp. 1-10.**
7. **Mark Yunovich, N.G.T., *AC Corrosion: Corrosion Rate and Mitigation Requirements.* Corrosion 2004, NACE, Houston, Texas, Paper No. 04206, 2004, pp. 1-18., 2004.**
8. **Lars Vendelbo Nielsen and K.V. Nielsen, M.A.B.B., HNG I/S; Henrik Breuning-Madsen, University of Copenhagen; Peter Cohn, DONG AS; Henrik Rosenberg, Balslev Consulting Engineers AS, *AC Induced Corrosion in Pipelines: Detection, Characterization and Mitigation.* NACE International, 2004.**
9. **Fernandes, S.Z., S.G. Mehendale, and S. Venkatachalam, *Influence of AC on Corrosion Kinetics for Carbon Steel, Zinc and Copper.* Corrosion 2005, NACE, Houston, Texas, Paper No. 05189, 2005, pp. 1-5, 2005.**
10. **Zhang, R., P.R. Vairavanathan, and S.B. Lalvani, *Perturbation method analysis of AC-induced corrosion.* Corrosion Science, 2008. 50(6): p. 1664-1671.**
11. **Büchler, M.a.H.G.S., *Investigation of Alternating Current Corrosion of Cathodically Protected Pipelines: Development of a Detection Method, Mitigation Measures, and a Model for the Mechanism.* Corrosion, 2009. 65(9): p. 578-586.**
12. **Belland, E., *Alternating Current Corrosion of Pipeline Steel.* Preliminary project work, Norwegian University of Science and Technology (NTNU), Trondheim, 2010.**
13. **Bosch, R.W. and W.F. Bogaerts, *A theoretical study of AC-induced corrosion considering diffusion phenomena.* Corrosion Science, 1998. 40(2-3): p. 323-336.**

Appendix A

Program: FE-10
Comment: Low alloy steel
Single spark(s)

FE-117169

10.03.2011 09:51:59

Elements: Concentration

Sample No: laagkarbon
Sample Id: 1

Quality:
Operator: SA

No	C %	Si %	Mn %	P %	S %	Cr %	Mo %	Ni %
1	0.0097	<0.0016	0.2147	0.0059	0.0078	0.0240	<0.0017	0.0432
2	0.0125	<0.0016	0.4073	0.0057	0.0076	0.0228	<0.0017	0.0430
3	0.0101	<0.0016	0.2170	0.0047	0.0076	0.0233	<0.0017	0.0419
4	0.0136	<0.0016	0.2143	0.0047	0.0071	0.0227	<0.0017	0.0413
5	0.0082	<0.0016	0.2165	0.0038	0.0072	0.0236	<0.0017	0.0417

No	Al %	Co %	Cu %	Nb %	Ti %	V %	Pb %	Sn %
1	0.0406	0.0142	0.0145	0.0015	0.0006	0.0029	<0.0034	<0.0014
2	0.0396	0.0140	0.0151	0.0015	0.0006	0.0021	<0.0034	<0.0014
3	0.0402	0.0136	0.0150	0.0019	0.0007	0.0031	<0.0034	<0.0014
4	0.0398	0.0143	0.0153	0.0017	0.0009	0.0032	<0.0034	<0.0014
5	0.0399	0.0142	0.0146	0.0018	0.0006	0.0034	<0.0034	<0.0014

No	Zr %	Ca %	B %	Zn %	Fe %	CE %
1	0.0024	0.0003	0.0011	0.0035	<99.6	0.0548
2	0.0026	0.0002	0.0011	0.0028	<99.4	0.0892
3	0.0029	0.0002	0.0011	0.0030	<99.6	0.0555
4	0.0027	0.0004	0.0009	0.0026	<99.6	0.0582
5	0.0029	0.0003	0.0009	0.0027	<99.6	0.0537

Program: FE-10
Comment: Low alloy steel
Average and RSD (n=5)

FE-117169

10.03.2011 09:52:53

Elements: Concentration

Sample No: laagkarbon
Sample Id: 1

Quality:
Operator: SA

	C %	Si %	Mn %	P %	S %	Cr %	Mo %	Ni %
$\bar{x}$	0.0108	<0.0016	0.2540	0.0050	0.0075	0.0233	<0.0017	0.0422
s	0.0022	0.0025	0.0857	0.0008	0.0003	0.0005	0.0031	0.0008
sr	20.157	158.502	33.754	16.942	3.967	2.326	183.976	1.966

	Al %	Co %	Cu %	Nb %	Ti %	V %	Pb %	Sn %
$\bar{x}$	0.0400	0.0141	0.0149	0.0017	0.0007	0.0029	<0.0034	<0.0014
s	0.0004	0.0003	0.0003	0.0002	0.0001	0.0005	0.0012	0.0008
sr	0.959	1.922	2.081	12.573	19.636	17.106	35.251	58.096

	Zr %	Ca %	B %	Zn %	Fe %	CE %
$\bar{x}$	0.0027	0.0003	0.0010	0.0029	<99.6	0.0622
s	0.0002	0.0001	0.0001	0.0004	0.0856	0.0151
sr	7.962	27.615	12.706	12.622	0.086	24.356

Figure A.1: Chemical composition determined by optical emission spectroscopy. Sheet 1.

Program: FE-10
Comment: Low alloy steel
Single spark(s)

FE-117169

10.03.2011 09:51:42

Elements: Concentration

Sample No: laagkarbon
Sample Id: 1

Quality:
Operator: SA

No	C %	Si %	Mn %	P %	S %	Cr %	Mo %	Ni %
1	0.0097	<0.0016	0.2147	0.0059	0.0078	0.0240	<0.0017	0.0432
2	0.0125	<0.0016	0.4073	0.0057	0.0076	0.0228	<0.0017	0.0430
3	0.0101	<0.0016	0.2170	0.0047	0.0076	0.0233	<0.0017	0.0419
4	0.0136	<0.0016	0.2143	0.0047	0.0071	0.0227	<0.0017	0.0413
5	0.0082	<0.0016	0.2165	0.0038	0.0072	0.0236	<0.0017	0.0417

No	Al %	Co %	Cu %	Nb %	Ti %	V %	Pb %	Sn %
1	0.0406	0.0142	0.0145	0.0015	0.0006	0.0029	<0.0034	<0.0014
2	0.0396	0.0140	0.0151	0.0015	0.0006	0.0021	<0.0034	<0.0014
3	0.0402	0.0136	0.0150	0.0019	0.0007	0.0031	<0.0034	<0.0014
4	0.0398	0.0143	0.0153	0.0017	0.0009	0.0032	<0.0034	<0.0014
5	0.0399	0.0142	0.0146	0.0018	0.0006	0.0034	<0.0034	<0.0014

No	Zr %	Ca %	B %	Zn %	Fe %	CE %
1	0.0024	0.0003	0.0011	0.0035	<99.6	0.0548
2	0.0026	0.0002	0.0011	0.0028	<99.4	0.0892
3	0.0029	0.0002	0.0011	0.0030	<99.6	0.0555
4	0.0027	0.0004	0.0009	0.0026	<99.6	0.0582
5	0.0029	0.0003	0.0009	0.0027	<99.6	0.0537

Figure A.2: Chemical composition determined by optical emission spectroscopy. Sheet 2.

Appendix B

Table B.1: Table showing estimated corrosion currents [mA/cm^2] at various rotational speeds and AC-current densities.

AC current density [A/m^2]	175 RPM			350 RPM		
	Parallel 1	Parallel 2	Average	Parallel 1	Parallel 2	Average
0	1,40E-04	1,20E-04	1,30E-04	1,80E-04	4,00E-04	2,90E-04
100	1,20E-04	1,30E-04	1,25E-04	2,00E-04	2,10E-04	2,05E-04
150	1,40E-04	1,40E-04	1,40E-04	1,50E-04	2,00E-04	1,75E-04
220	1,50E-04	1,80E-04	1,65E-04	3,10E-04	1,90E-04	2,50E-04
500	1,50E-04	1,30E-04	1,40E-04	2,20E-04	2,20E-04	2,20E-04

Table B.2: Cathodic tafel slopes at various AC-current densities and rotational speeds.

	175 RPM		350 RPM	
AC current density [A/m^2]	Parallel 1	Parallel 2	Parallel 1	Parallel 2
0	-0,28	-0,30	-0,38	-
100	-0,25	-0,24	-0,28	-
150	-0,24	-0,23	-0,29	-0,31
220	-0,24	-0,27	-0,29	-0,25
500	-0,17	-0,18	-0,24	-0,25

Appendix C

Appendix C includes current density response transients from the LPR measurements and the corresponding R_p' values. Note that the R_p' [$\Omega \cdot cm^2$] is the R_p [Ω] multiplied by the sample surface area. The R_p [Ω] value is based on total current, not current density, and corrected for IR-drop prior calculation of R_p' [$\Omega \cdot cm^2$].

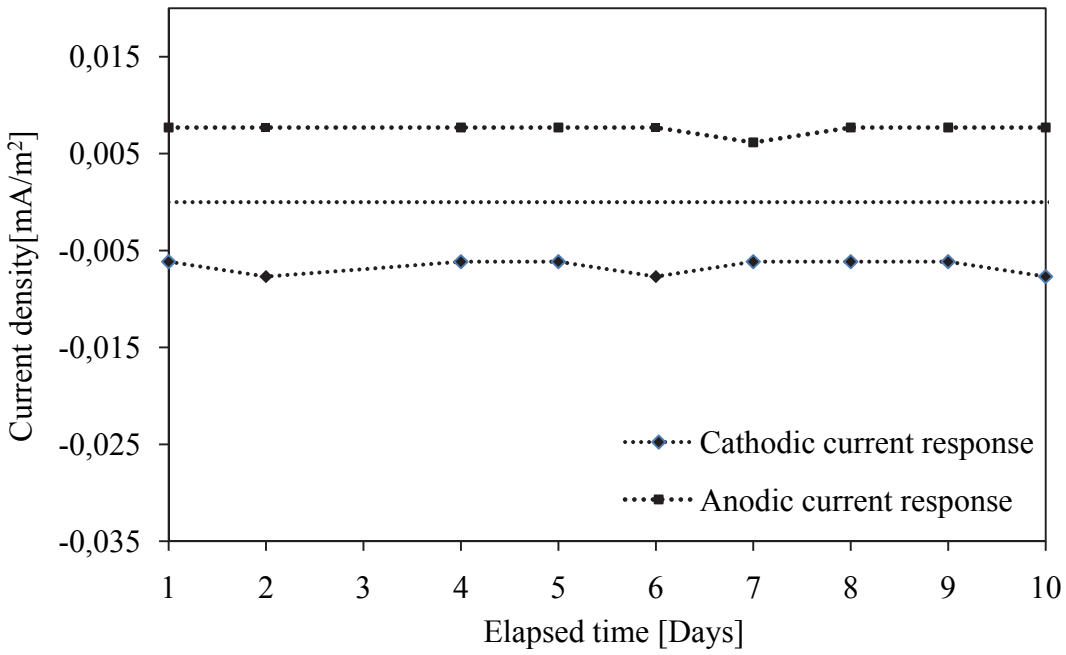

Figure C.1: LPR measurement transient from weight loss sample without induced AC.

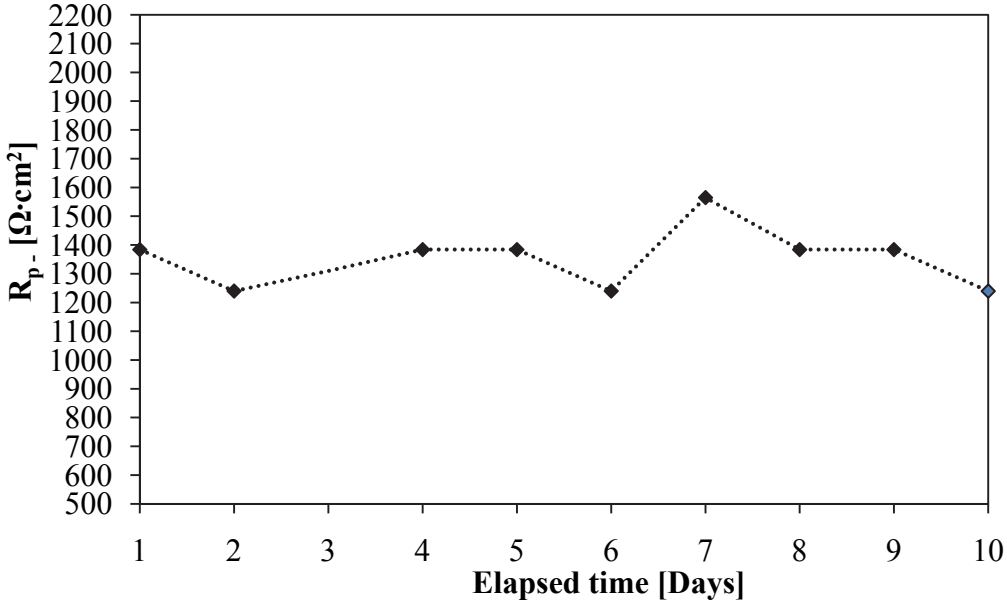

Figure C.2: R_p'transient from weight loss sample without induced AC-current.

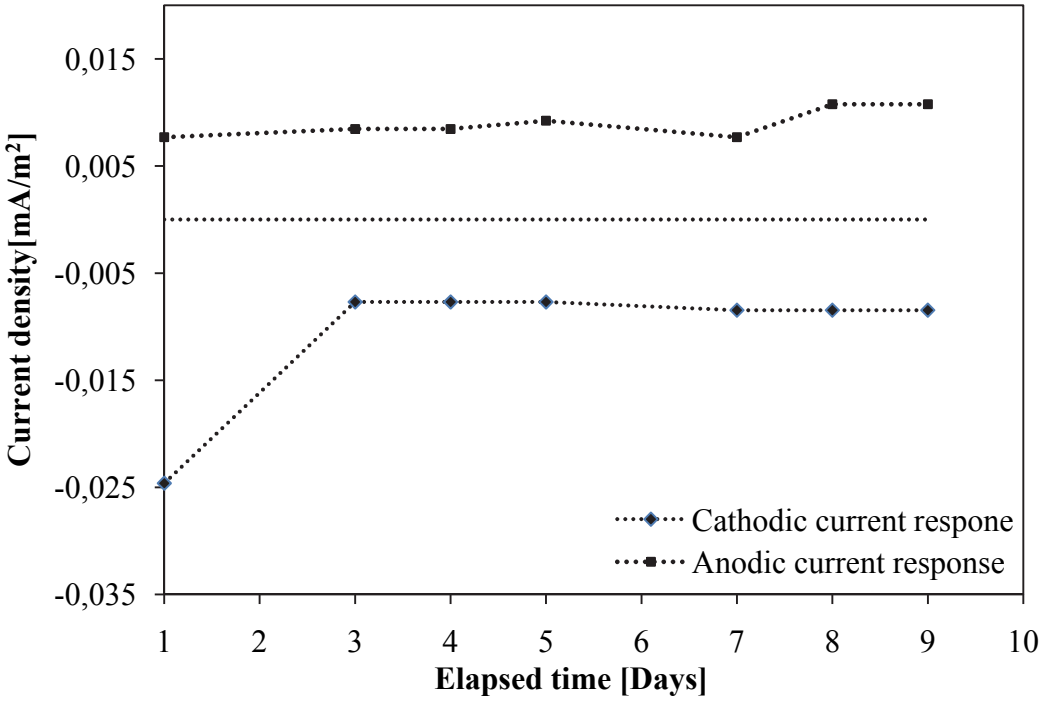

Figure C.3: LPR measurement transient from weight loss sample exposed to 50 A/m^2.

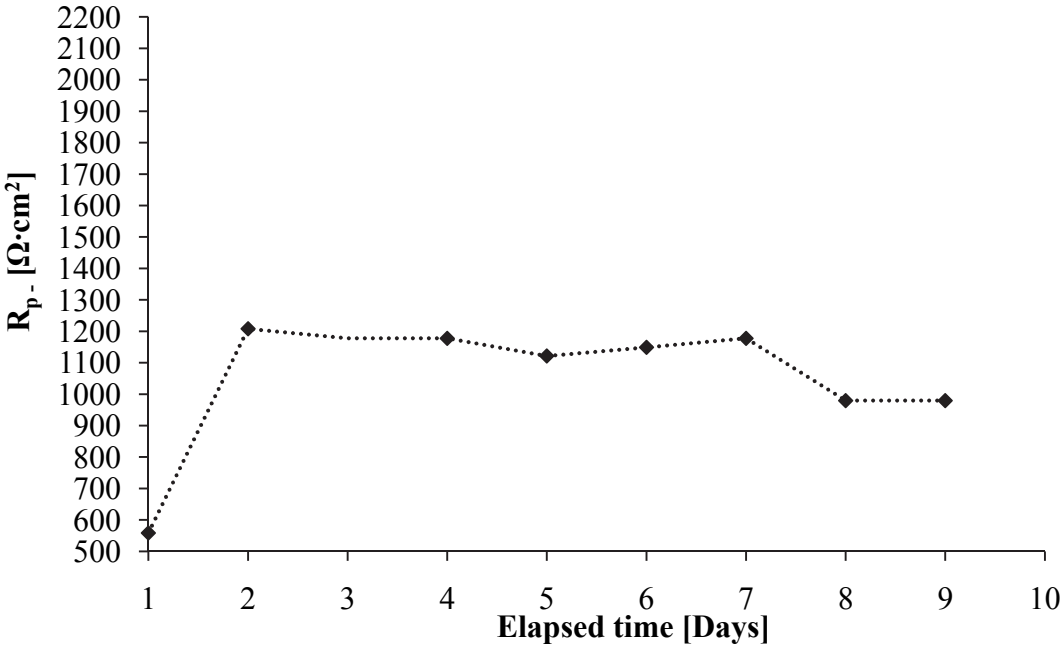

Figure C.4: R_p'transient from weight loss sample exposed to 50 A/m^2.

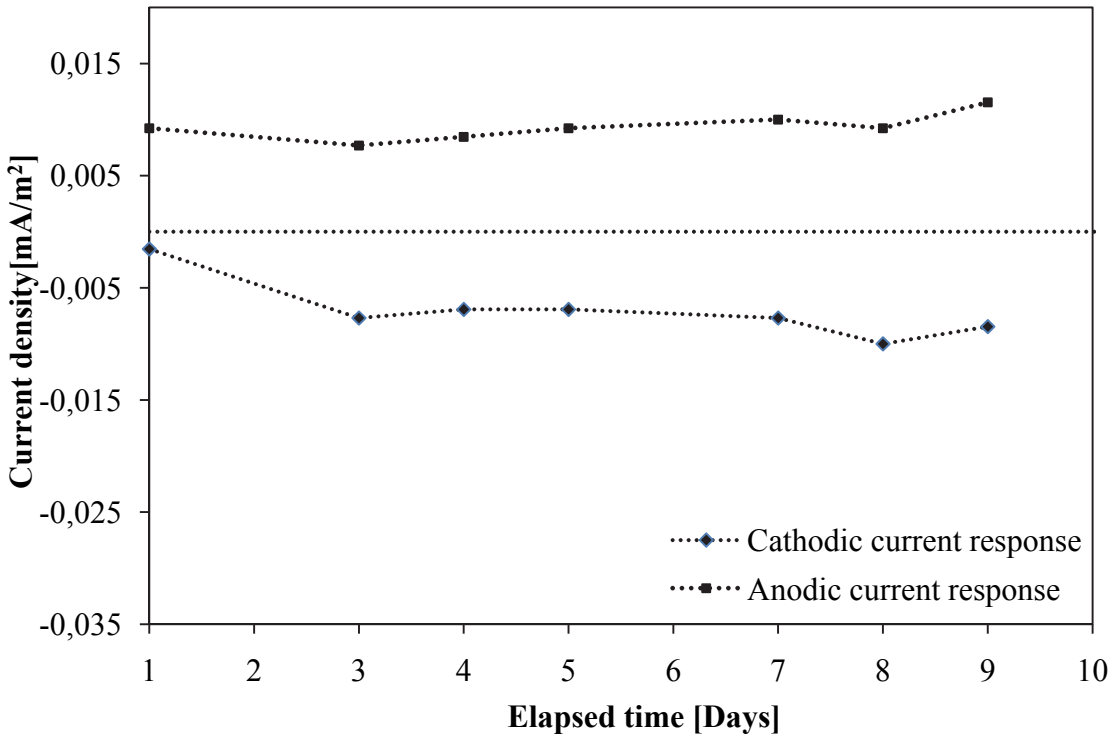

Figure C.5: LPR measurement transient from weight loss sample exposed to 75 A/m^2.

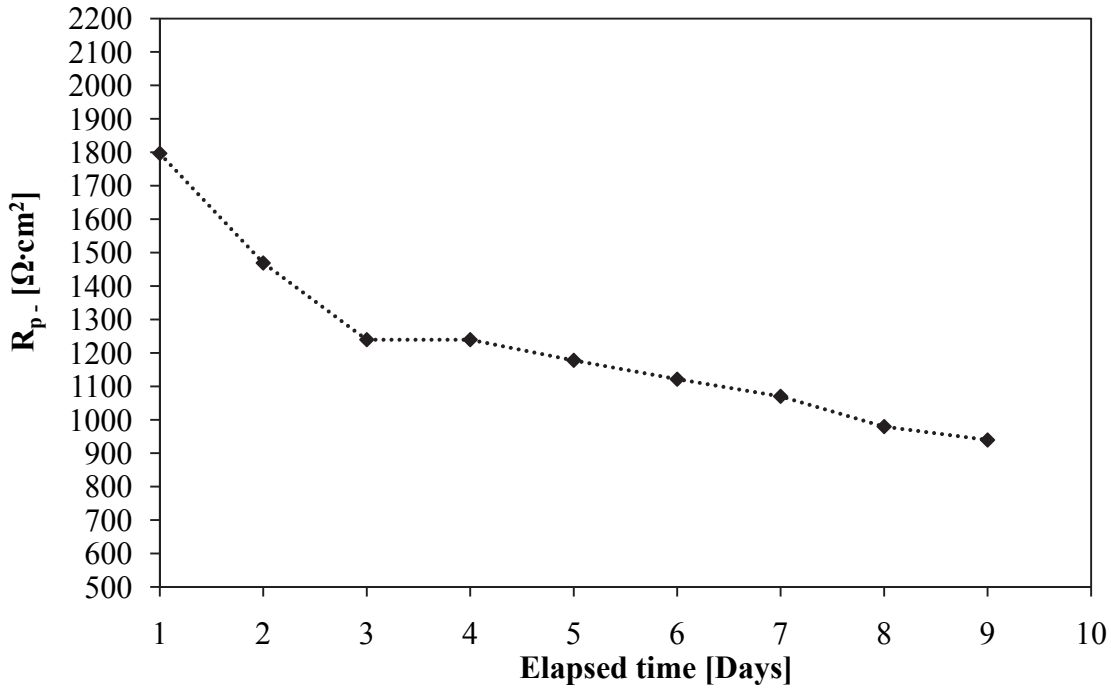

Figure C.6: R_p'transient from weight loss sample exposed to 75 A/m^2.

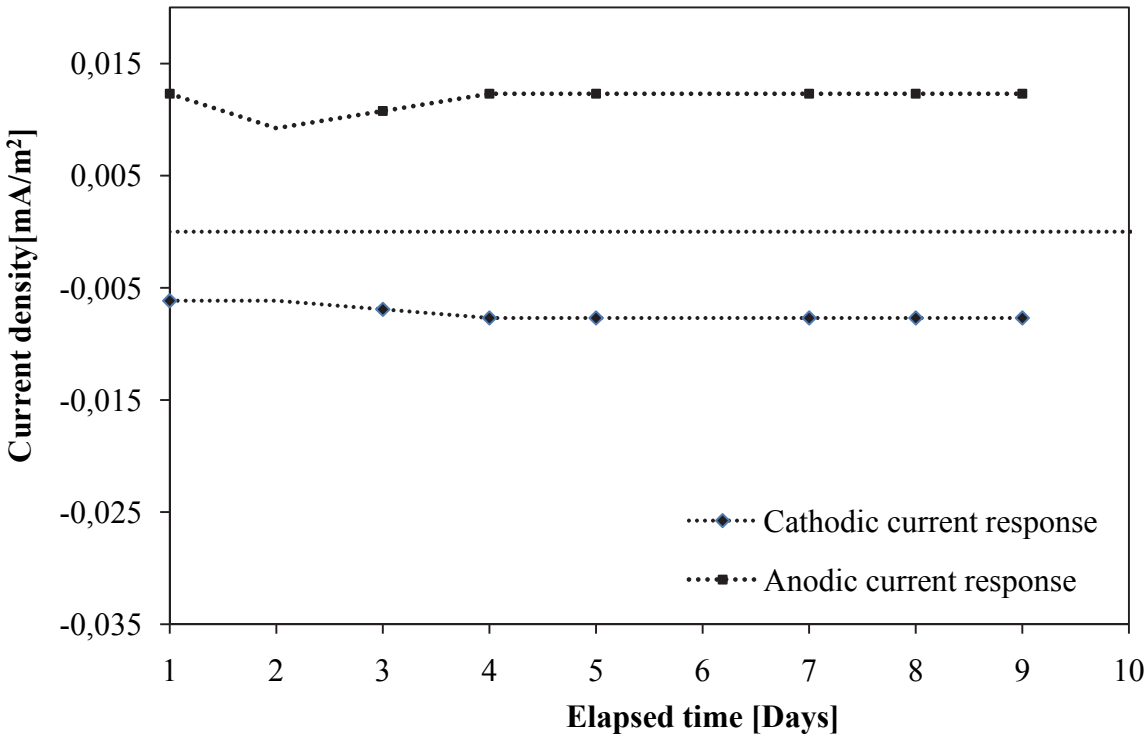

Figure C7: LPR measurement transient from weight loss sample exposed to 100 A/m^2.

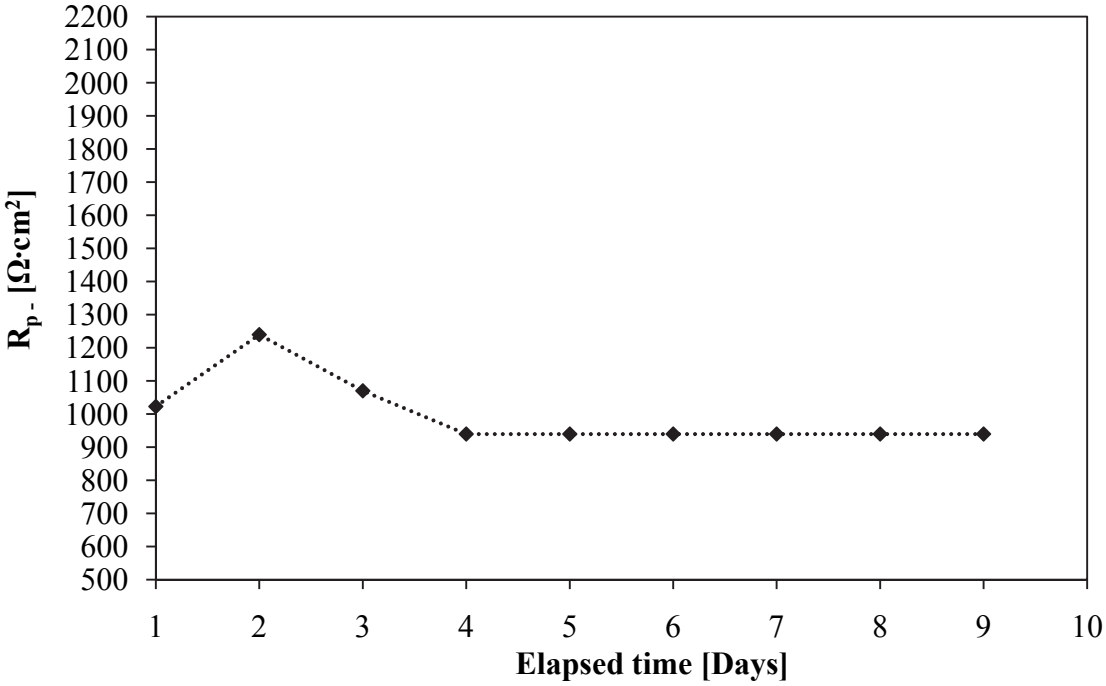

Figure C.8: R_p'transient from weight loss sample exposed to 100 A/m^2.

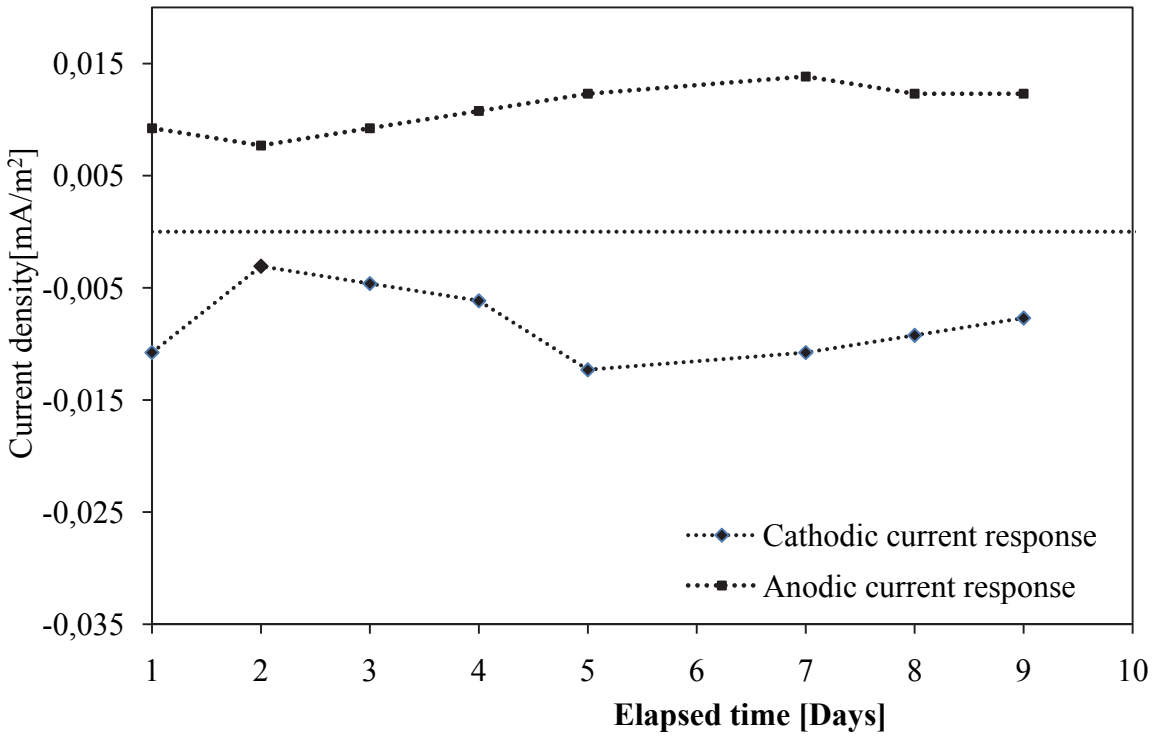

Figure C.9: LPR measurement transient from weight loss sample exposed to 150 A/m^2.

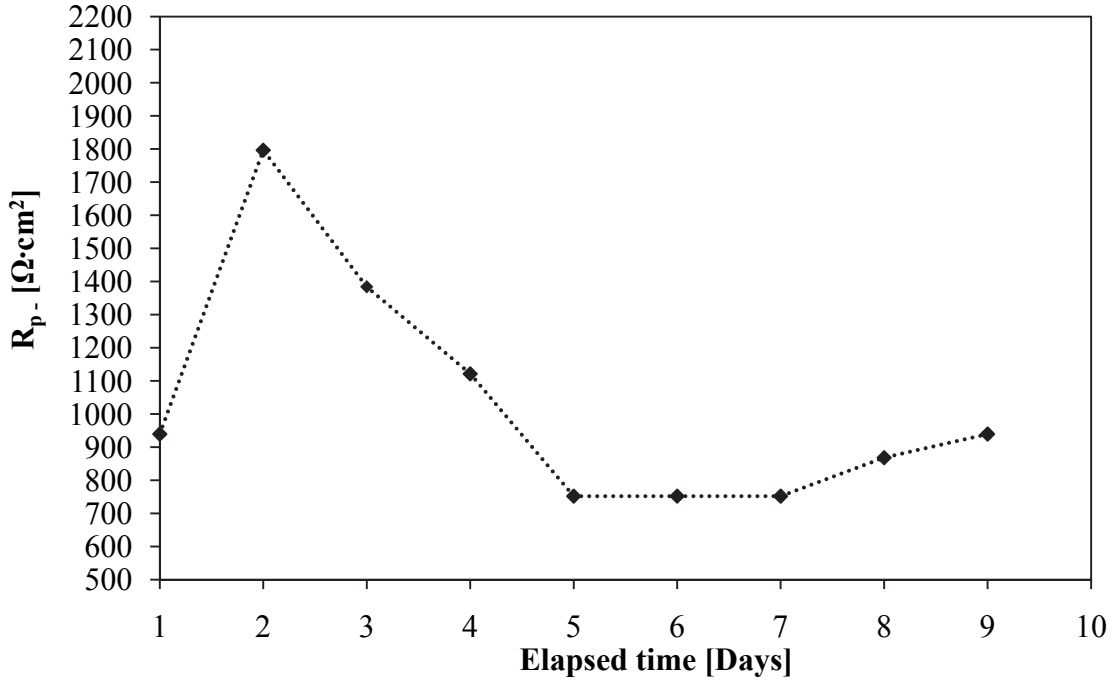

Figure C.10: R_p' transient from weight loss sample exposed to 150 A/m^2.

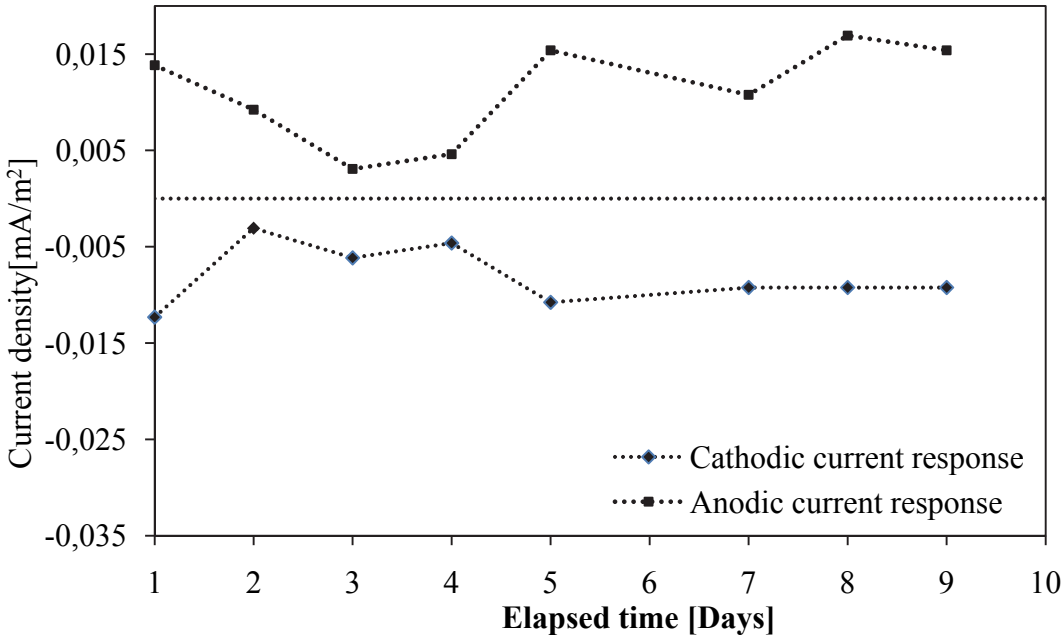

Figure C.11: LPR measurement transient for weight loss sample exposed to 220 A/m^2. ansient from

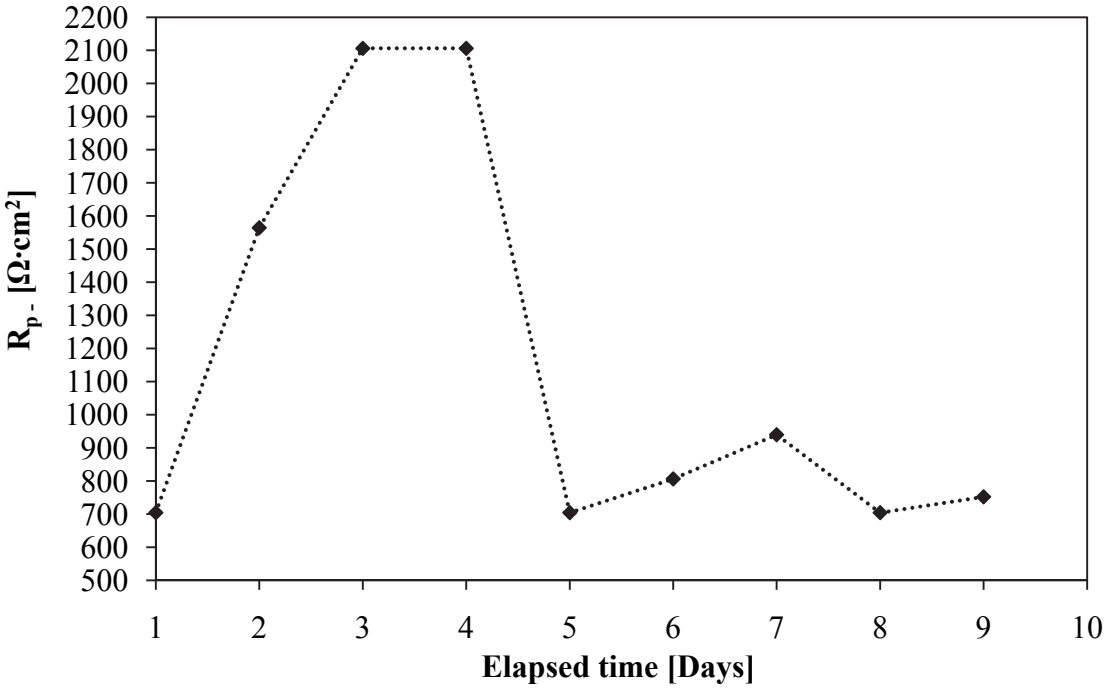

Figure C.12: R_p' transient from weight loss sample exposed to 150 A/m^2.

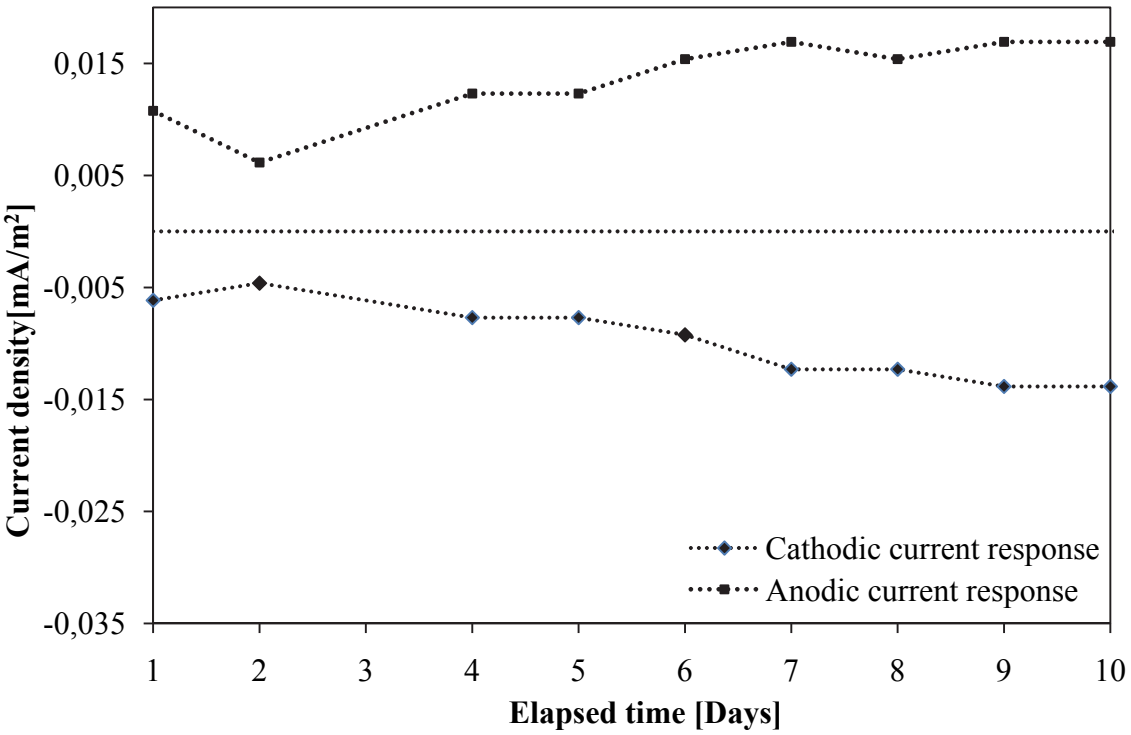

Figure C13: LPR measurement transient from weight loss sample exposed to 500 A/m^2.

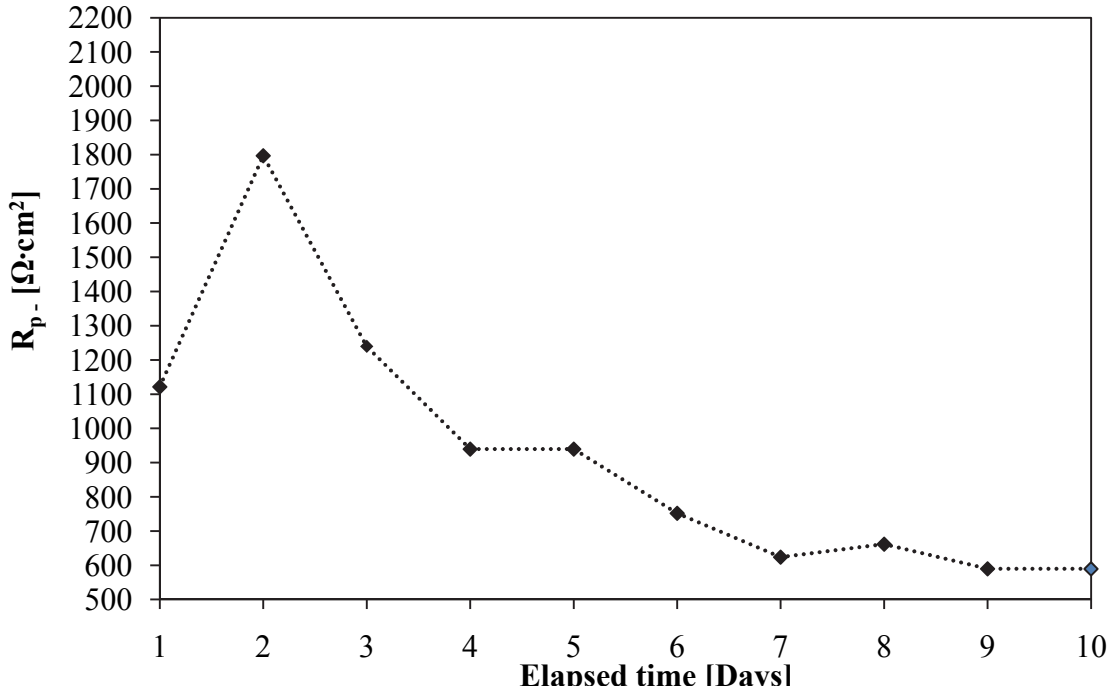

Figure C.14: R_p' transient from weight loss sample exposed to 500 A/m^2.